Intra-mitochondrial protein degradation alleviates alpha-synuclein seeding and Abeta 42 aggregation

Running title: Intra-mitochondrial protein degradation

Janin Lautenschläger[1*], Sara Wagner-Valladolid[1], Amberley D. Stephens[1], Ana Fernández-Villegas[1], Colin Hockings[1], Ajay Mishra[1], James D. Manton[2], Marcus J. Fantham[3], Meng Lu[1], Eric J. Rees[2], Clemens F. Kaminski[3], Gabriele S. Kaminski Schierle[1*]

[1] Molecular Neuroscience Group, Department of Chemical Engineering and Biotechnology, University of Cambridge, West Cambridge Site, Philippa Fawcett Drive, Cambridge, CB3 0AS, UK; [2] Quantitative Imaging Group, Department of Chemical Engineering and Biotechnology, University of Cambridge, West Cambridge Site, Philippa Fawcett Drive, Cambridge, CB3 0AS, UK; [3] Laser Analytics Group, Department of Chemical Engineering and Biotechnology, University of Cambridge, West Cambridge Site, Philippa Fawcett Drive, Cambridge, CB3 0AS, UK

* Corresponding authors:

Janin Lautenschläger, Gabriele S. Kaminski Schierle

Email: janin.lautenschlaeger@gmail.com, gsk20@cam.ac.uk

Molecular Neuroscience Group, Department of Chemical Engineering and Biotechnology

University of Cambridge, West Cambridge Site, Philippa Fawcett Drive, Cambridge, CB3 0AS, UK

Character count: 55 270

Abstract

Mitochondria have long been implicated in Parkinson's disease, ever since the discovery that inhibitors of the mitochondrial complex I can lead to dopaminergic neuron death. We report here that intra-mitochondrial protein degradation alleviates (PFF)-induced alpha-synuclein seeding, highly relevant for the spreading of alpha-synuclein pathology. We find that interference with mitochondrial protein import as well as intra-mitochondrial proteases aggravates the aggregation profile and indeed, alpha-synuclein shows themselves as intra-mitochondrial protein. We further demonstrate that mitochondrial protein degradation is relevant for the aggregation of Abeta 42, suggesting that mitochondria are directly linked to disturbances in cytosolic protein homeostasis of aggregation prone proteins. Taken together, this draws a new picture of how mitochondrial dysfunction is involved in neurodegenerative diseases and provokes new therapeutical approaches.

Keywords: alpha-synuclein / Abeta 42 / mitochondria / neurodegeneration / seeding

Introduction

Mitochondria have long been implicated in Parkinson's disease (PD), ever since the discovery that inhibitors of the mitochondrial complex I can lead to dopaminergic neuron death (Langston *et al*, 1983; Burns *et al*, 1983; Betarbet *et al*, 2000; Greenamyre *et al*, 2001; Sherer *et al*, 2003). Furthermore, mutation of phosphatase and tensin homolog (PTEN)-induced kinase 1 (PINK1) or parkin, leading to failure of mitophagy, link mitochondrial dysfunction and familial PD. A connection between both, alpha-synuclein aggregation and mitochondrial dysfunction, is suggested by recent studies highlighting that alpha-synuclein aggregation is increased in PINK1 and parkin mutant iPS-cells and parkin transgenic mice (Chung *et al*, 2016; Lu *et al*, 2009).

An important factor influencing PD pathophysiology is the fact that alpha-synuclein aggregates can spread from cell to cell, which has been described as prion-like behavior (Kordower & Brundin, 2009; Stopschinski & Diamond, 2017). Indeed, also in vitro small fibrillar seeds, constituting misfolded alpha-synuclein, transfer from one cell to another and induce aggregation of normally folded endogenous alpha-synuclein (Luk *et al*, 2009; Pinotsi *et al*, 2016). Since the seeding of alpha-synuclein is understood as a driving force for disease progression, we here aimed to investigate if mitochondrial dysfunction and which mechanisms of mitochondrial dysfunction in particular influence the alpha-synuclein seeding propensity.

Using the preformed fibril (PFF)-induced alpha-synuclein aggregation model we show that mitochondrial dysfunction clearly aggravated PFF-induced seeding, however an artificial

increase in cytosolic calcium, oxidative stress or inhibition of complex I were not able to reproduce the enhanced seeding of alpha-synuclein. We demonstrate that the seeding propensity is dependent on intra-mitochondrial proteostasis, and identified that the high temperature requirement protein A2 (HtrA2), a mitochondrial intermembrane protease, and mitochondrial protein import are crucial in determining the level of alpha-synuclein seeding. We further show that alpha-synuclein is found in mitochondria, supporting our hypothesis that mitochondria play an important role in alpha-synuclein degradation.

Results

The preformed fibril (PFF) model mimics alpha-synuclein seeding in disease

The seeding of alpha-synuclein aggregation was modelled by the preformed fibril (PFF) assay as initially developed by Luk et al. (Luk *et al*, 2009), and proved to be of substantial use in studying alpha-synuclein aggregation in vitro as well as in vivo (Pinotsi *et al*, 2016; Luk *et al*, 2009, 2012; Peelaerts *et al*, 2015; Thakur *et al*, 2017). Here, SH-SY5Y cells overexpressing YFP-alpha-synuclein were incubated for 4 hours with PFFs made from unlabeled human recombinant alpha-synuclein (Supplementary Fig. 1), and cultured for another 3 days to allow seeding of alpha-synuclein aggregation (Fig. 1A). While YFP-alpha-synuclein overexpressing cells per se not display any Lewy-body-like inclusions, fine filamentous inclusions build up from YFP-alpha-synuclein are seen by structured illumination microscopy (SIM) upon PFF incubation (Fig. 1B). This model system reflects a late disease state in which the seeds for aggregation are already present and thus has a particular focus on factors influencing alpha-

synuclein seeding. YFP-alpha-synuclein inclusions stain positive for ubiquitin and p62, which are both characteristic markers found in Lewy bodies of human disease (Luk *et al*, 2009) (Fig. 1C and D).

Mitochondrial dysfunction increases alpha-synuclein seeding

From our previous study, we have seen that alpha-synuclein strongly interacts with calcium, leading to conformational changes at the calcium binding domain at the C-terminus, but also at the NAC-region, which suggests a potential influence of calcium on the aggregation propensity of alpha-synuclein. Consistently, increased calcium significantly aggravated alpha-synuclein nucleation in vitro (Lautenschläger *et al*, 2018). However surprisingly, when cells were treated with BAPTA-AM, a well-known specific calcium chelator, PFF-induced alpha-synuclein seeding was drastically increased (Fig. 2A). This is in contrast to what has been expected, since BAPTA-AM is supposed to decrease cytosolic calcium and was reported previously to alleviate KCl-induced alpha-synuclein aggregation (Follett *et al*, 2013). In our study, we found that BAPTA-AM did decrease cytosolic calcium in the SH-SY5Y cells, but only transiently. The effect was already compensated for treatments of 1 hour and 5 hours (Fig. 2B), suggesting that the effect on alpha-synuclein seeding is mediated via a different pathway. Both the ester form BAPTA, BAPTA-AM, as well as the active BAPTA itself did not increase the aggregation of alpha-synuclein in vitro (t50 125.6+/-8.6 and 122.6+/-7.2 vs. 116.6+/-11.1) (Fig. 2C), indicating that the effect of BAPTA in the PFF assay results from a cellular response. In fact, we found that BAPTA-AM had a direct impact on mitochondria, inducing organelle fragmentation as determined by SIM imaging (Fig. 2D). This cellular response upon BAPTA-AM

122 treatment is related to an increase of ER-dependent mitochondrial fission and has been
123 reported previously (Friedman *et al*, 2011).
124
125 This led us to hypothesize that mitochondrial dysfunction per se could influence alpha-
126 synuclein seeding. Indeed, also carbonyl cyanide 4-(trifluoromethoxy)phenylhydrazone
127 (FCCP), a mitochondrial uncoupler that dissipates the mitochondrial membrane potential and
128 thus leads to mitochondrial dysfunction, increased YFP-alpha-synuclein seeding (Fig. 2E).
129 Similarly, FCCP did not increase alpha-synuclein aggregation in vitro (t50 117.0+/-9.8 vs.
130 115.6+/-10.1), confirming that its effect in the PFF assay was the result of a cellular response
131 rather than a direct interaction of the two (Fig.2F).
132
133 **Classical downstream effectors of mitochondrial dysfunction are unable to influence alpha-**
134 **synuclein seeding**
135
136 Mitochondrial dysfunction is known to culminate in complex I inhibition, cytosolic calcium
137 increase and oxidative stress, therefore we artificially mimicked these downstream effectors
138 of mitochondrial dysfunction. 1-methyl-4-phenylpyridinium (MPP^+), the active metabolite of
139 1-methyl-4-phenyl-1,2,3,6-tetrahydropyridine (MPTP) was used to inhibit complex I of the
140 electron transport chain, ionomycin, an ionophore, was used to increase cytosolic calcium
141 concentration via calcium influx through the plasma membrane, and menadione was used to
142 induce reactive oxygen species (ROS) generation via redox-cycling (Criddle *et al*, 2006). These
143 chemicals were applied during the incubation with PFFs, and also during the 3 day incubation
144 until seeding was evaluated. However, none of these treatments provoked increased YFP-
145 alpha-synuclein seeding (Fig. 3A). Measuring cytosolic ATP levels, calcium levels and ROS

generation we show that treatment with MPP^+, menadione and ionomycin led to either higher or comparable levels of ATP, calcium or ROS, respectively, than after treatment with either FCCP or BAPTA-AM, suggesting that complex I inhibition, cytosolic calcium increase and oxidative stress do not aggravate alpha-synuclein seeding per se (Fig. 3B and C).

Inhibition of HtrA2 increases alpha-synuclein seeding

The effect of BAPTA-AM on alpha-synuclein seeding was more pronounced compared to FCCP, since one hour pre-incubation with BAPTA-AM already aggravated alpha-synuclein seeding, however not the one hour pre-incubation with FCCP (Fig. 2A and 2E). Though, FCCP treatment led to increased mitochondrial fragmentation compared to BAPTA-AM (Fig. 3D and E), suggesting that there is no direct correlation between mitochondrial fragmentation and alpha-synuclein seeding propensity. BAPTA-AM has been reported to inhibit proteases (Da Cruz *et al*, 2011; Wang *et al*, 2001; Ray *et al*, 2002), which is mediated via the blocking of intracellular calcium transients required to regulate protease activity (Demartino *et al*, 1982; Mellgren, 1987). This could demonstrate a more enduring effect of BAPTA-AM and thus led us to investigate the effect of mitochondrial proteostasis on alpha-synuclein seeding.

Mitochondria present a very unique compartment for the folding of proteins, because the vast majority of proteins are imported as linear polypeptides that are folded once inside. Moreover, reactive oxygen species constantly arise due to oxidative phosphorylation which occurs at the inner mitochondrial membrane. Thus, it is not surprising that mitochondria are well equipped with chaperones and also proteases to control mitochondrial protein

homeostasis (Quirós *et al*, 2015). Intriguingly, mitochondrial proteases have recently been found to regulate the dissolution of cytosolic protein aggregates after heat shock (Ruan *et al*, 2017) indicating that they are not only responsible for the maintenance of intra-mitochondrial proteins as previously assumed. We thus aimed to test if inhibition of mitochondrial proteases could influence alpha-synuclein seeding using the PFF assay as a model system. To test the role of the Lon-protease, a protease residing in the mitochondrial matrix, cells were treated with the Lon-inhibitor CDDO-Me (Gibellini *et al*, 2015). To investigate the role of high temperature requirement protein A2 (HtrA2/Omi), a protease residing in the mitochondrial intermembrane space (IMS), cells were treated with the inhibitor UCF-101 (Cilenti *et al*, 2003).

Both mitochondrial protease inhibitors significantly increased PFF-induced alpha-synuclein seeding (Fig. 4A). The effect upon inhibition of the Lon protease was lower than seen upon inhibition of HtrA2, although the Lon protease had previously been found to have the highest impact on the dissolution of aggregates after heat shock (Ruan *et al*, 2017). Interestingly, HtrA2 had previously been linked to PD (Strauss *et al*, 2005; Bogaerts *et al*, 2008; Unal Gulsuner *et al*, 2014), however genetic studies were not fully conclusive since pathological mutations of HtrA2 had also been reported in control subjects. Though, HtrA2 was encountered to be a constituent of protein aggregates in human alpha-synucleinopathies (Kawamoto *et al*, 2008; Strauss *et al*, 2005).

Inhibition of mitochondrial protein import enhances alpha-synuclein seeding

We isolated mitochondria from wild-type adult rat brain and demonstrated that they were positive for alpha-synuclein, and that proteinase K digestion was not able to degrade all alpha-

synuclein, indicating that some of the protein also resided within the organelle. If, however, 0.1% Triton X-100 was added during the proteinase K digestion, alpha-synuclein was fully degraded as the detergent fully solubilizes mitochondrial membranes (Fig. 4B and C). This result could be further supported by transmission electron microscopy (TEM) of YFP alpha-synuclein SH-SY5Y cells, displaying alpha-synuclein staining inside mitochondria (Fig. 4D and Supplementary Fig. 2). Mitochondrial import of alpha-synuclein had been reported previously, but had been critically debated (Devi *et al*, 2008). However, several recent studies demonstrate that alpha-synuclein interacts with the mitochondria import receptor Tom20 (Di Maio *et al*, 2016; Ryan *et al*, 2018; Martínez *et al*, 2018). Thus, we hypothesized that inhibition of mitochondrial protein import might have a similar effect on alpha-synuclein seeding as the inhibition of proteases. Using Mitoblock-6, a small molecule inhibitor of protein translocation into mitochondria (Dabir *et al*, 2013), we observed increased alpha-synuclein seeding using the PFF assay (Fig. 4E), thus arguing for a direct role of mitochondrial proteostasis on alpha-synuclein homeostasis.

Mitochondrial proteostasis regulates β-amyloid 42 aggregation

The above discussed mechanisms of mitochondrial proteostasis could have wider implications, and thus may not be unique to alpha-synuclein as suggested previously (Ruan *et al*, 2017). Therefore, we wanted to test if our findings on alpha-synuclein aggregation would be consistent within another aggregation model. To test this, we used a stable HEK cell line overexpressing Aβ42-mCherry via a tetracycline inducible expression system. After induction, these cells were treated for 24 hours with the different mitochondrial inhibitors. We found that both, FCCP and BAPTA-AM, increased the aggregation of native β-amyloid 42 (Aβ42), with

BAPTA-AM again having a more pronounced effect (Fig. 5A). In addition, inhibition of either HtrA2 with UCF-101 or of mitochondrial protein import with mitobloCK-6 significantly increased Aβ42 aggregation similar to our observations using alpha-synuclein (Fig. 5B and C). In addition, we have overexpressed HtrA2 in HEK Aβ42-mCherry cells and show that Aβ42 aggregation is 50 % decreased by 50 % compared to control conditions demonstrating that HtrA2 plays a significant role in regulating the proteostasis of amyloidogenic proteins (Fig. 5D).

In-vitro aggregation of β-amyloid 42 is influenced by HtrA2

To investigate the direct effect of mitochondria on protein aggregation in an isolated system, we analyzed Aβ42 protein in vitro aggregation via fluorescence lifetime of fluorescently labelled protein (Chan *et al*, 2013; Kaminski Schierle *et al*, 2011). For this, Aβ42 containing 50 % Hylite^{TM} Fluor 488 labelled Aβ42 was incubated for 2 hours at room temperature, the fluorescence lifetime of Hylite^{TM} Fluor 488 dropped from 3380 +/- 93 ps to 3003 +/- 97 ps (timepoint 0 compared to timepoint 2 hrs, p = 0.0025, df 25) which is directly correlated with protein aggregation (Chen *et al*, 2017; Schierle *et al*, 2014). However, in the presence of isolated rat brain mitochondria, almost no drop in the fluorescence lifetime occurred (timepoint 0 = 3538+/- 15 ps compared to timepoint 2hrs = 3502 +/- 5 ps, ns, Fig. 6A). Note, the lifetime is also higher at timepoint 0, which is due to the immediate aggregation of Aβ42 in the control group. If the mitochondria were pre-incubated with UCF-101 which is inhibiting the HtrA2 protease, the fluorescence lifetime of Hylite^{TM} Fluor 488 decreased over the 2 hour time period (timepoint 0 = 3523 +/- 16 ps compared to 2hrs = 3429 +/- 20 ps, p = 0.0009, df

241 27, Fig. 6B) which supports the hypothesis that mitochondria influence protein aggregation
242 via proteolysis, however other proteases besides HtrA2 may also be involved.
243
244
245 **Discussion**
246
247 This study demonstrates that a decline in mitochondria fitness, whether by loss of
248 mitochondrial integrity or by inhibiting the intramitochondrial protein homeostasis increases
249 alpha-synuclein seeding. This is in accordance with the finding that mutations in genes
250 encoding for PINK1 and parkin enhance alpha-synuclein aggregation, since defects in
251 mitophagy equate to decreased mitochondrial fitness (Chung *et al*, 2016; Lu *et al*, 2009).
252 However, as we have not found a direct contribution of downstream effects of mitochondrial
253 dysfunction, we propose a direct link between mitochondrial protein uptake and degradation
254 and alpha-synuclein seeding.
255
256 So far the effect of amyloidogenic proteins on mitochondria has been interpreted as a
257 secondary pathological hallmark. It has been shown that alpha-synuclein as well as Aβ
258 exacerbate mitochondrial dysfunction in vitro as well as in vivo (Cha *et al*, 2012; Subramaniam
259 *et al*, 2014; Rui & Zheng, 2016). Alpha-synuclein and Aβ have been reported to inhibit the
260 uptake of mitochondrial proteins and Aβ has been also shown to inhibit preprotein maturation
261 (Di Maio *et al*, 2016; Cenini *et al*, 2016; Mossmann *et al*, 2014). We here pose the question of
262 whether the import of amyloidogenic proteins into mitochondria is a physiological
263 phenomenon or not. On one side, proteins might be imported into mitochondria since they
264 exert a specific function as recently discussed for alpha-synuclein (Ludtmann *et al*, 2016). On

the other side, protein degradation via mitochondrial proteases within the organelle could demonstrate a general mechanism connected to cellular stress, as discussed recently for cytosolic protein dissolution after heat shock (Ruan *et al*, 2017). We have shown that alpha-synuclein is contained within mitochondria, the prerequisite for its degradation within the organelle. This is in accordance with previous papers, which have shown the uptake and preferential interaction of alpha-synuclein with mitochondria in vitro (Devi *et al*, 2008; Reeve *et al*, 2015; Robotta *et al*, 2014). Furthermore, alpha-synuclein has recently been found to interact with the mitochondrial import machinery, especially Tom20 as reported from three independent groups (Di Maio *et al*, 2016; Ryan *et al*, 2018; Martínez *et al*, 2018).

Interestingly, in our study inhibition of HtrA2 had the most significant effect on alpha-synuclein seeding. From the literature, we would have expected the strongest effect to occur via inhibition of the Lon protease, since it was found to have the most prominent contribution to the degradation of heat shock induced protein aggregation and is commonly described as the “master” protease (Ruan *et al*, 2017; Bezawork-Geleta *et al*, 2015; Gur & Sauer, 2008). Furthermore, the Lon protease resides in the matrix of mitochondria, while HtrA2 is confined to the intermembrane space. However, HtrA2 has previously been genetically linked to Parkinson’s disease (Strauss *et al*, 2005; Bogaerts *et al*, 2008; Westerlund *et al*, 2011; Unal Gulsuner *et al*, 2014; Chao *et al*, 2015) and a neuroprotective role of the protein has been suggested, since mice with mutant HtrA2 or HtrA2 knock out suffer from neurodegeneration (Jones *et al*, 2003; Martins *et al*, 2004). However, this has been puzzling so far, since HtrA2 has been attributed a pro-apoptotic function in somatic cells, and thus a neuroprotective effect would have be expected upon knock out (Vaux & Silke, 2003). Thus, a direct role of

HtrA2 via its protease function is likely and is supported by the finding that HtrA2 interacts with presenilin-1 and Aβ (Gray *et al*, 2000; Gupta *et al*, 2004; Liu *et al*, 2005; Park *et al*, 2004).

While we have not found a direct link between alpha-synuclein seeding and mitochondrial downstream effectors, such as complex I inhibition, ROS and calcium increase, this does not mean that they do not play an important role during the course of the disease. We strongly support the notion that calcium plays a role in PD, possibly affecting mitochondrial fitness when specific neuronal subtypes are subjected to increased calcium concentrations over long time periods as recently shown (Chan *et al*, 2007). That there has not been a direct effect of calcium on alpha-synuclein seeding was initially puzzling, since we and others have shown that calcium can accelerate alpha-synuclein aggregation in vitro (Nath *et al*, 2011; Lautenschläger *et al*, 2018). However, we have shown that calcium preferentially affected the lag time of alpha-synuclein aggregation kinetics, while the elongation was only slightly increased (Lautenschläger *et al*, 2018). Thus, if calcium only has an effect on the nucleation kinetics of alpha-synuclein aggregation we would not necessarily expect to observe an effect on alpha-synuclein seeding in cells (Buell *et al*, 2014).

It has been reported lately that mitochondrial heat shock proteins and proteases are upregulated in patients with AD, and also in patients with mild cognitive impairment (Sorrentino *et al*, 2017), indicating that these pathways are induced early on in disease. Furthermore, the translocase of the outer membrane 40 (Tom 40), the pore forming protein of the mitochondrial protein import complex, has been genetically linked to Alzheimer's and Parkinson's disease (Gottschalk *et al*, 2014). This demonstrates that mechanisms of mitochondrial proteostasis are extremely interesting to understand in more detail in order to

312 develop new concepts for therapeutical approaches. Taken together, our study shows that
313 mitochondrial proteostasis is an important factor influencing the aggregation of alpha-
314 synuclein and Aβ42, extending the concept of mitochondria as guardian in cytosol (MAGIC)
315 (Ruan *et al*, 2017) to the degradation of amyloidogenic proteins and drawing a new picture on
316 how mitochondria contribute to neurodegeneration.
317
318
319 **Material and Methods**
320 ***Human cell culture***
321 *Human neuroblastoma cells* (SH-SY5Y) were obtained from the European Collection of Cell
322 Cultures (ECACC, Sigma-Aldrich, Dorset, UK) and grown in a 1:1 minimal essential medium
323 (MEM) (Sigma-Aldrich) and nutrient mixture F-12 Ham (Sigma-Aldrich) supplemented with 15
324 % FBS, 1 % non-essential amino-acids, 2 mM GlutaMAX and 1 % antibiotic-antimycotic (all
325 Thermo Fisher Scientific, Epsom, UK). SH-SY5Y cells stably expressing YFP-alpha-synuclein
326 were obtained by lentiviral transfection using 3rd generation lentiviruses (Addgene constructs:
327 12251, 12253, 12259) (Dull *et al*, 1998). Human wildtype alpha-synuclein was inserted into
328 EYFP plasmid (pEYFP-N1) using a 5 amino acid linker (sequence: GCACCGGTCGCCACC)
329 between the C-terminus of alpha-synuclein and N-terminal EYFP. Alpha-synuclein-EYFP was
330 then cloned into the pLJM1 backbone for lentiviral expression (Addgene: 19319) (Sancak *et al*,
331 2008). For the preformed fibril (PFF) assay 50,000 cells were plated in MatTek dishes (P35G-
332 1.5-14-C, MatTek Corporation, Ashland, US). For analysis of mitochondrial fragmentation cells
333 were plated at 20,000 per well in NuncTM Lab-TekTM II Chambered Coverglass (8 well,
334 155409, Thermo Fisher Scientific).

Flp-InTM T-RExTM 293 cell line (Invitrogen), a derivative of HEK293 cells containing a stably integrated FRT site and a TetR repressor, were used to generate stable cell lines expressing either mCherry or Aβ42-mCherry (pcDNA3.3-mCherry, pcDNA3.3-Ab42-mCherry) under the Flp-InTM expression vector as described previously (Wu *et al*, 2014; Lu *et al*, 2019). Cells were maintained in DMEM high glucose media (Sigma-Aldrich) supplemented with 10% fetal bovine serum (FBS), 2 mM glutaMAX, and 1 % antibiotic-antimycotic (all Thermo Fisher Scientific). Cells were grown at 37°C under a 5% CO2 atmosphere. Cells were plated at 35 000 cells per well in NUNC 24 well plates, and construct expression was induced for 3 days using media above with 1 µg/mL tetracycline (Sigma Aldrich) added. All cell lines were tested for mycoplasma contamination using the MycoAlertTM PLUS mycoplasma detection kit (Lonza, Walkersville). For transient transfection of HtrA2 (Plun-Favreau *et al*, 2007) electroporation with the NEON transfection system was used (settings: 1050 V, 30 ms, 2 pulses; Thermo Fisher Scientific). pcDNA3-HtrA2-FLAG was a gift from L. Miguel Martins (Addgene plasmid # 15938; http://n2t.net/addgene:15938; RRID:Addgene_15938).

Cell were imaged on a widefield microscope with IX83 frame (Olympus, Tokyo, Japan), HPLS343 plasma light source (Thorlabs, Newton, US), and Clara interline CCD camera (Andor, Belfast, UK), controlled by Micromanager (Edelstein *et al*, 2014). Respective filter cubes for YFP (excitation 500 nm, dichroic mirror 515 nm, emission 535 nm), RFP (excitation 560 nm, dichroic mirror 585 nm, emission 630 nm) and DAPI (excitation 350 nm, dichroic mirror 400 nm, emission 460 nm) were used. Images for YFP-alpha-synuclein aggregation and DAPI were taken with an Olympus Plan Apo U 60x/1.42 oil objective lens. Imaging was done randomly by automated acquisition of a grid of 7x7 images per area. Aggregates were identified by their fibrillar nature, cell nuclei were counted using FIJI (Schindelin *et al*, 2012). For Aβ42-mCherry aggregation images were taken with an Olympus LUCPlanFLN 20x/0.45 air objective lens.

Aggregates were identified using the Thresholder plugin in ICY (de Chaumont *et al*, 2012). The cell surface area was evaluated using the HK-Means plugin for ICY (Arai & Barakbah, 2007).

Alpha-synuclein fibrils

Human wild-type (WT) alpha-synuclein was expressed in Escherichia coli One Shot® BL21 STAR™ (DE3) (Invitrogen, Thermo Fisher Scientific) cells using plasmid pT7-7 and purified using ion exchange on a HiPrep Q FF 16/10 anion exchange column (GE Healthcare, Uppsala, Sweden) (Huang *et al*, 2005). Alpha-synuclein was then further purified on a HiPrep Phenyl FF 16/10 (High Sub) hydrophobic interaction column (GE Healthcare) (Campioni *et al*, 2014). Purification was performed on an ÄKTA Pure (GE Healthcare). Monomeric protein was dialyzed against 20 mM phosphate buffer pH 7.2, lyophilized in a LyoQuest 85 freeze-dryer (Telstar, Spain), and stored at -80 °C.

Alpha-synuclein fibrils were produced by diluting alpha-synuclein monomer solution to a concentration of 150 µM in 20 mM phosphate buffer, pH 7.2. Samples were incubated at 37°C for 5 days in 0.5 mL Protein Lobind tubes (Eppendorf, Hamburg, Germany) under continuous rotation at maximum speed (UVP HB-1000 Hybridizer, Fisher Scientific). Fibrils were diluted 1:1 with 20 mM phosphate buffer, pH 7.2 to a final volume of 200 µL and sonicated (Digital Sonifier® SLPe, model 4C15, Branson, Danbury, USA) with six 10 sec pulses at 70 % amplitude and 10 sec pause after each sonication pulse. Sonicated fibrils were aliquoted, exposed to UV light for 30 min and frozen immediately after at -80C.

Alpha-synuclein fibrils were imaged by atomic force microscopy (AFM) (BioScope Catalyst microscope, Bruker AXS GmbH, Fitchburg, USA). Fibrils at an equivalent monomer concentration of 5 µM were deposited for 30 min on High Performance cover glass (PN 474030-9020-000, Carl Zeiss Ltd.), cleaned for 30 min with 1 M KOH (Fluka, Bucharest,

383 Romania) and coated for 30 min with 0.01 % poly-L-Lysine beforehand (P4707, Sigma).
384 Samples were rinsed 5 times with deionized water and dried under nitrogen flow. AFM data
385 were acquired using PeakForce Quantitative Nanomechanical Property mapping mode with
386 ScanAsyst-Fluid+ probes (Bruker AXS GmbH). Images were flattened and exported using
387 NanoScope Analysis software, version 1.8.
388
389 ***Preformed fibril (PFF) assay***
390 For the induction of alpha-synuclein seeding, YFP-alpha-synuclein overexpressing SH-SY5Y
391 cells were incubated with sonicated preformed alpha-synuclein fibrils as described by Luk et
392 al. (Luk *et al*, 2009). Briefly, cells plated in MatTek dishes were washed with Neurobasal
393 medium and subsequently changed to 500 µL Neurobasal medium supplemented with 2 %
394 B27 and 0.5 mM GlutaMAX (all Thermo Fisher Scientific). Cells were preincubated for 1 hour,
395 either using 0.2 % DMSO for control or the respective treatment (see cell treatments below).
396 8 µL of PFFs were diluted with 32 µL HBSS (HBSS minus calcium and magnesium, no phenol
397 red, 14175-053, Thermo Fisher Scientific) and mixed briefly 5 times. Fibrils were added to the
398 bottom of the BioPORTER tube (BioPORTER® Protein Delivery agent, BP502424, Gelantis, San
399 Diego, USA), mixed 5 times and incubated for 5 min at room temperature, then vortexed for
400 5 sec at 600 rpm (Stuart™ Scientific SA8 vortex mixer, Sigma-Aldrich). 460 µL OptiMEM
401 medium (Thermo Fisher Scientific) were added to the BioPORTER tube plus the respective
402 treatments and mixed 5 times. The PFF mixture was added dropwise to the cells, settled and
403 then incubated for 4 hours at 37°C and 5 % CO_2. Final monomer equivalent concentration of
404 preformed fibrils was 600 nM.
405

After 4 hours cells were washed twice with 1 ml Neurobasal medium and changed subsequently to 2 mL of retinoic acid medium made of 1:1 minimal essential medium (MEM) (Sigma-Aldrich) and nutrient mixture F-12 Ham (Sigma-Aldrich) supplemented with 5 % FBS, 1 % non-essential amino-acids, 2 mM GlutaMAX and 1 % antibiotic-antimycotic (all Thermo Fisher Scientific) and 1 µM retinoic acid (Sigma-Aldrich) plus treatments if indicated and incubated for another 3 days to allow aggregate formation. Cells were fixed for 10 min using 4 % formaldehyde in PBS supplemented with 4 % sucrose, 5 mM $MgCl_2$ and 10 mM EGTA, pH 7.4 (Marchenko & Flanagan, 2007), stained with Hoechst 33342 (Molecular Probes, Thermo Fisher Scientific) 1:2000 in PBS for 30 min.

Cell treatments

Chemical used for the treatment of cells were prepared as followed, with final dilution made with the respective culture medium. Carbonyl cyanide 4-(trifluoromethoxy)phenylhydrazone (FCCP, Abcam, Cambridge, UK) 1 mM in DMSO, N-Methyl-4-phenylpyridinium Iodide (MPP+, Sigma-Aldrich) 10 mM in water, ionomycin (ab120370, Abcam) 10 mM and 1 mM in DMSO, 2-Deoxyglucose (Sigma-Aldrich) 0.5 M in water, menadione (Sigma-Aldrich) 1.5 mM in DMSO, BAPTA-AM (ab120503, Abcam) 2.5 mM in DMSO, BAPTA (ab144924, Abcam) 1 mM in water, CDDO-Me (Sigma-Aldrich) 1 mM in DMSO, UCF-101 (Sigma-Aldrich) 10 mM in DMSO and MitobloCK-6 (Focus Biomolecules) 5 mM in DMSO.

Immunofluorescence

Cells were fixed as described above, blocking and permeabilization were performed using 5 % donkey serum in 0.05 % Tween-20 in phosphate buffered saline (PBS) for 1 h. Primary antibodies were incubated overnight at 4°C, followed by 5 washes with PBS. Secondary antibodies were incubated for 1 hour at room temperature, followed by 5 washes with PBS. As primary antibodies anti-Ubiquitin antibody, clone Apu2 (05-1307, 1:200, Millipore, Watford, United Kingdom), anti-Ubiquitin-binding protein p62, clone 2C11 (SQSTM1, 1:200, Abnova, Taipei, Taiwan) and anti-FLAG® M2 antibody (F1804, 1:200, Sigma-Aldrich) were used. As secondary antibodies anti-rabbit and anti-mouse Alexa Fluor®647, and anti-mouse Alexa Fluor®568 (A-21245, A-21236 and A-11031 from life technologies) were used. Samples were kept in PBS containing 5 mM sodium azide (Sigma-Aldrich).

Structured illumination microscopy (SIM)

Structured illumination images were collected on a custom built Structured Illumination Microscopy (SIM) setup which has been described in detail (Young *et al*, 2016). A 60×/1.2NA water immersion lens (UPLSAPO 60XW, Olympus) focused the structured illumination pattern onto the sample. This lens also captured the samples' fluorescence emission light before imaging onto a sCMOS camera (C11440, Hamamatsu). Laser excitation wavelengths used were 488 nm (iBEAM-SMART-488, Toptica), 561 nm (OBIS 561, Coherent), and 640 nm (MLD 640, Cobolt). Respective emission filters were BA 510-550 (Olympus), BrightLine FF01-600/37, and BrightLine FF01-676/29 (Semrock, New York, US). Imaging was done in fixed cells or live cells, as indicated. Images were acquired using custom SIM software (HCImage, Mamamatsu Corporation, Sewickley, US). Nine raw images were collected at each plane and each color. FairSIM plugin in FIJI was used to reconstruct images (Müller *et al*, 2016).

450

451 ***FLIM measurements of cytosolic calcium, H_2O_2, and ATP***

452 Fluorescence lifetime microscopy (FLIM) was carried out on a custom-built Time-Correlated
453 Single Photon Counting (TCSPC) system using a super-continuum laser (SC450, Fianium) with
454 a pulse repetition rate of 40 MHz, a confocal scanning unit (FluoView 300, Olympus) coupled
455 with an inverted microscope frame (IX70, Olympus), and a time-correlated single photon
456 counting system (Becker & Hickl GmbH) as described in detail before (Chen *et al*, 2015). The
457 excitation wavelength was selected by using an acousto-optic tunable filter (AOTFnC-400.650,
458 Quanta Tech) and respective excitation filters (to improve the wavelength selection), and
459 emission fluorescence was imaged through respective emission filters. The data acquisition
460 time was 200s for each FLIM image (10 cycles, 20s per cycle). The photon detection rate was
461 kept below 2% of the laser repetition rate in order to avoid photon pile-up.

462 For cytosolic calcium measurements SH-SY5Y cells were incubated with Oregon GreenTM 488
463 BAPTA-1, AM (Thermo Fisher Scientific) for 45 min at 1 µM concentration. Excitation was set
464 to 475 nm, excitation filter BrightLine FF01-474/27 (Semrock), and emission filter BrightLine
465 FF01-525/39 (Semrock) were used. For measurement of H2O2 and ATP SH-SY5Y cells were
466 transiently transfected with the respective sensor using electroporation with the NEON
467 transfection system (settings: 1100 V, 50 ms, 1 pulse; Thermo Fisher Scientific). Hyper
468 (Belousov *et al*, 2006) was used to measure cytosolic hydrogene peroxide, excitation was set
469 to 470 nm, same excitation and emission filters as for Oregon GreenTM 488 BAPTA-1 were
470 used. Ateam1.03 (Imamura *et al*, 2009; Kotera *et al*, 2010) was used to measure ATP levels,
471 excitation was set to 435 nm, excitation filter BrightLine FF01-434/17 (Semrock), and emission
472 filter BrightLine FF01-470/28 (Semrock) were used. ATeam1.03-nD/nA/pcDNA3 was a gift
473 from Takeharu Nagai (Addgene plasmid # 51958; http://n2t.net/addgene:51958;

RRID:Addgene_51958). For ATP measurements cells were subjected to media containing 10 mM 2-Deoxyglucose to inhibit glycolysis. Lifetime of the FRET donor was analyzed by the FLIMfit software tool developed at Imperial College London (Görlitz *et al*, 2017; Warren *et al*, 2013).

ThT Assay

The aggregation of alpha-synuclein in vitro was measured by Thioflavin T (ThT) assay. Briefly, 50 µL of 100 µM alpha-synuclein with 10 µM fresh ThT added, was incubated for 7 days with 1% DMSO as a control, 10 µM FCCP, 10 µM BAPTA-AM, or 10 µM BAPTA. Assays were performed in NUNC™ black 384-well plates with optical flat bottom (142761, Thermo Fisher Scientific) which were sealed with an Ampliseal transparent microplate sealer (Greiner Bio-One GmbH). Plates were incubated with orbital shaking at 300 rpm for 5 minutes before each read every hour at 37 °C for 170 cycles. The readings of ThT fluorescence intensity were taken using excitation at 440 nm and emission at 480 nm, collected from the bottom up with 20 flashes per well and a gain setting of 1300 (FLUOstar Omega, BMG Labtec GmbH, Ortenberg, Germany). Experiments were repeated three times with four replicates for each condition.

Mitochondrial fragmentation

To label mitochondria SH-SY5Y cells were incubated over night with 1:1000 CellLight™ Mitochondria-RFP (Thermo Fisher Scientific) and imaged by SIM or a widefield microscope for quantification. Images were taken randomly by automated imaging of a grid, images were analyzed from 3 biological repeats. Mitochondrial length was evaluated using the NIEL Mito algorithm (Lautenschläger *et al*, 2015; Herbert *et al*, 2014).

497

498 ***Animals***

499 Adult female Sprague Dawley rats were supplied by Charles River UK Ltd., Scientific, Breeding
500 and Supplying Establishment, registered under Animals (Scientific Procedures) Act 1986, and
501 AAALAC International accredited. All animal work conformed to guidelines of animal
502 husbandry as provided by the UK Home Office. Animals were sacrificed under schedule 1;
503 procedures that do not require specific Home Office approval. Animal work was approved by
504 the NACWO and University of Cambridge Ethics Board.

505

506 ***Mitochondrial isolation and Western blot analysis***

507 Mitochondria were isolated from adult rat brain by differential centrifugation using
508 mitochondria isolation kit for tissue (ab110168, abcam). Western blot for alpha-synuclein was
509 performed using 4–12% Bis-Tris gels (Life Technologies), the protein was transferred onto 0.45
510 µm Millipore PVDF membrane (Fisher Scientific, Loughborough, UK) and subsequently fixed
511 using 4% formaldehyde + 0.1% glutaraldehyde in PBS (both Sigma-Aldrich) (Lee & Kamitani,
512 2011). As primary antibody α-Synuclein (D37A6) XP® Rabbit mAb was used (1:1000 dilution,
513 #4179, CST, Leiden, Netherlands). An enhanced chemoluminescence (ECL)-horse radish
514 peroxidase (HRP) conjugated secondary antibody (NA934V, 1:1000 dilution, GE Healthcare,
515 Uppsala, Sweden) and SuperSignal West Femto Chemiluminescent Substrate (Thermo Fisher
516 Scientific) were used to probe the membrane, which was exposed using a G:BOX (Syngene,
517 Cambridge, UK). Western blots were analyzed in FIJI (Schindelin *et al*, 2012).

518

519 ***TEM***

SH-SY5Y cells and SH-SY5Y cells overexpressing YFP-alpha-synuclein were cultured in 6 well plates (Greiner Bio-One GmbH) at 350 000 per well. After reaching confluency cells were washed with 0.9% NaCl (Sigma-Aldrich) twice and incubated with 8% formaldehyde in 0.05 M sodium cacodylate buffer (Paraformaldehyd from Merck, Darmstadt, Germany) pH 7.4 for 2h at 4°C. Cells were scraped from 6 wells and centrifuged for 10 min at 3500 g. Cells were washed 5 times in 0.05 M sodium cacodylate buffer, 3 times in deionized water, and incubated with 2 % uranyl acetate in 0.05 maleate buffer pH 5.2 (both BDH Chemicals Ltd., Dorset, UK) overnight at 4°C. Cells were washed again and dehydrated at increasing ethanol concentrations (1x 50% EtOH, 3x 70% EtOH, 3x 95 % EtOH, 3x 100% EtOH, 3x 100 % dry EtOH; 5 min in each, Sigma-Aldrich). Cells were resuspended in LRW resin (LR White Resin, London Resin (Hard), Agar Scientific, Stansted, UK) mixed 50/50 with dry 100% EtOH and incubated overnight at room temperature. The following day, cells were spun down, and resuspended in pure LRW for 2 days, where LRW was exchanged twice. Cells were centrifuged at 13000 g to form a firm pellet, which was transferred to size 2 gelatine embedding capsules (TAAB, Aldermaston, UK) containing LRW resin. Gelatine capsules were covered with a glass coverslip to exclude any air and the resin was cured at 60°C for 2 days. Gelatine capsule were removed and ultrathin sections were cut using a Leica Ultracut E Ultramicrotome (Leica, Wetzlar, Germany) and placed on 400 mesh nickel/formvar film grids (EM Resolutions). Sections were stained with Anti-GFP antibody (ab6556, Abcam) in blocking solution (2 % BSA (BBITM solutions, Crumlin, UK) in 10 mM TRIS (Sigma-Aldrich) buffer pH 7.4 containing 0.001% Triton-X100 (Calbiochem, San Diego, US) and 0.001% Tween20 (Sigma-Aldrich) at 1:100 overnight. After washing, sections were incubated with goat anti rabbit 10 nm gold secondary antibody (BBITM solutions) in blocking solution at 1:200 for 1 hour. Sections were washed with washing buffer (same as above omitting BSA), deionized water and left for drying overnight. Post-

staining included 2% uranyl acetate in 50 % methanol for 30 sec, followed by washing with 50 % methanol and 30 sec staining in Reynold's lead citrate (lead nitrate from BDH Biochemicals Ltd., Trisodiumcitrate from Sigma-Aldrich). Grids were rinsed thoroughly with deionized water and dried before imaging. Grids were imaged in a FEI Tecnai G2 electron microscope (Thermo Fisher Scientific) run at 200 keV using a 20 µm objective aperture, images were taken using an AMT V600 camera (AMT, Woburn, US).

In-vitro measurements of Aβ42 aggregation

Synthetic Aβ42 and Aβ42 Hilyte™ Fluor 488 (both from Anaspec, Seraing, Belgium) were prepared as previously described (Sum *et al*, 2016). Briefly, lyophilized Aβ42 (1 mg) was dissolved in ice cold trifluroacetic acid (200 mL), sonicated at 0 °C for 60 s and then lyophilized overnight. Ice cold 1,1,1,3,3,3-hexafluro-2-propanol (1 mL) was added, sonicated at 0 °C for 60 s and aliquoted as 20 µL units. The samples were lyophilized overnight and were stored at -80 °C until use. Lyophilized Aβ42 Hilyte™ Fluor 488 peptide (0.1 mg) was dissolved in 1% NH_4OH (200 µL) and sonicated for 60 s at 0 °C. The sample was aliquoted into 5 µL units, snap frozen in liquid nitrogen and stored at -80 °C. Immediately before the experiment unlabeled Aβ42 was prepared by adding first dimethyl sulfoxide (DMSO) (5% of total solvent volume), then sodium phosphate buffer (NaP buffer 50mM, pH 7.4) to reach a concentration of 20 µM. The solution was sonicated at 0 °C for 3 min and centrifuged at 13,400 rpm at 0 °C for 30 min. Then the sample was further diluted to 5 µM concentration with NaP buffer. Also the labelled Aβ42 Hilyte™ Fluor 488 was brought to 5 µM concentration in NaP buffer and both were mixed in 1:1 ratio. Samples were prepared on ice adding Aβ42, 1 mg/mL of purified mitochondria (preparation see above) and 20 µM UCF-101. Mitochondria isolation buffer and DMSO were added in control samples. 12 µL volume were pipetted in silicon gaskets (Thermo Fisher

Scientific, P24742) on a coverslip and measured at room temperature. Fluorescence lifetime measurements (FLIM) were carried out on a custom-built Time-Correlated Single Photon Counting (TCSPC) system as described above (see FLIM measurements of cytosolic calcium, H_2O_2, and ATP).

Statistics

Statistical analysis was performed using GraphPad Prism 6.07 (GraphPad Software, Inc., La Jolla, CA, USA). Values are given as mean ± SEM unless otherwise stated. Normal distribution was tested using Shapiro-Wilk test. Two-tailed unpaired t-test was used upon normal distribution, two-tailed Mann-Whitney U test was used when no normal distribution was given. For multiple comparisons either one-way ANOVA with Dunnett's post hoc correction upon normal distribution or Kruskal-Wallis test with Dunn's multiple comparison when no normal distribution was given were performed. Significance was considered at $p < 0.05$.

Data availability.

All relevant data are available from the corresponding authors.

Acknowledgements

We would like to thank Karin H. Muller and Jeremy N. Skepper for their help and input for the transmission electron microscopy study. We would like to thank Samantha Beck for establishing the YFP-alpha-synuclein SH-SY5Y cell line. J.L. was supported by a research fellowship from the Deutsche Forschungsgemeinschaft (DFG; award LA 3609/2-1). C.F.K. acknowledges funding from the UK Engineering and Physical Sciences Research Council (EPSRC). G.S.K.S. and C.F.K. acknowledge funding from the Wellcome Trust, the UK Medical Research Council (MRC), Alzheimer Research UK (ARUK), and Infinitus China Ltd. J.L. and A.D.S. acknowledge Alzheimer Research UK (ARUK) travel grants.

Author contributions

J.L., A.F.V. and A.M. contributed to alpha-synuclein PFF assay and cell work. J.L performed FLIM experiments and mitochondrial morphology analysis. A.D.S. performed alpha-synuclein in vitro work. J.L. and A.F.V. and C.H. contributed to Western blot analyses. J.L. performed TEM. J.L., S.W.V. and M.L. contributed to Aβ42 studies. J.M. and M.F. contributed to automated and SIM imaging. J.L. designed the experiments. J.L., C.F.K. and G.S.K.S. conducted the overall manuscript.

Conflict of interest

The authors declare no conflict of interest.

The Paper Explained

PROBLEM: Neurodegenerative diseases like Alzheimer's and Parkinson's disease put a high social and economic burden on modern societies. Since the early 1990s, protein aggregation is found as an overarching phenomenon of these diseases, however, we still do not understand why proteins start to undergo aggregation, particularly in sporadic cases of disease, which represent the majority.

RESULTS: Here, we demonstrate that the aggregation of proteins relevant to neurodegenerative diseases, like alpha-synuclein in Parkinson's disease and Amyloid-beta 42 in Alzheimer's disease, is alleviated by mitochondrial degradation of these proteins. We show that alpha-synuclein is contained within mitochondria and that the inhibition of mitochondrial uptake of proteins, as well as inhibition of protein degrading enzymes within the mitochondria, aggravate the seeding of alpha-synuclein aggregation. This implies that this mechanism is relevant to late disease stages, when alpha-synuclein aggregation is already initiated. Furthermore, we demonstrate that the aggregation of Abeta 42 is increased upon inhibition of these mechanisms and that aggregation can be decreased by overexpression of a mitochondrial protease. Taken together, this shows that mitochondrial protein degradation demonstrates a general mechanism influencing the homeostasis of aggregation prone proteins.

IMPACT: It was highlighted recently that mitochondria are able to degrade cytosolic proteins, however thus far it has only been speculated that this is the case for proteins relevant to neurodegeneration. Our results directly link mitochondrial dysfunction to protein aggregation, which could have major implication to explain the sporadic occurrence of neurodegenerative diseases upon a decline in mitochondrial fitness after chronic exposure to environmental toxins or aging per se.

638

639 **References**

640 Arai K & Barakbah AR (2007) Hierarchical K-means: an algorithm for centroids initialization
641 for K-means. *Rep. Fac. Sci. Engrg. Reports Fac. Sci. Eng. Saga Univ. Saga Univ.* **36:** 36–
642 125

643 Belousov V V, Fradkov AF, Lukyanov KA, Staroverov DB, Shakhbazov KS, Terskikh A V &
644 Lukyanov S (2006) Genetically encoded fluorescent indicator for intracellular hydrogen
645 peroxide. *Nat. Methods* **3:** 281–286

646 Betarbet R, Sherer TB, Mackenzie G, Garcia-osuna M, Panov A V & Greenamyre JT (2000)
647 Chronic systemic pesticide exposure reproduces features of Parkinson's disease. *Nat.*
648 *Neurosci.* **3:** 1301–1306

649 Bezawork-Geleta A, Brodie EJ, Dougan DA & Truscott KN (2015) LON is the master protease
650 that protects against protein aggregation in human mitochondria through direct
651 degradation of misfolded proteins. *Sci. Rep.* **5:** doi: 10.1038/srep17397 Available at:
652 http://www.nature.com/articles/srep17397

653 Bogaerts V, Nuytemans K, Reumers J, Pals P, Engelborghs S, Pickut B, Corsmit E, Peeters K,
654 Schymkowitz J, De Deyn PP, Cras P, Rousseau F, Theuns J & Van Broeckhoven C (2008)
655 Genetic variability in the mitochondrial serine protease HTRA2 contributes to risk for
656 Parkinson disease. *Hum. Mutat.* **29:** 832–840

657 Buell AK, Galvagnion C, Gaspar R, Sparr E, Vendruscolo M, Knowles TPJ, Linse S & Dobson CM
658 (2014) Solution conditions determine the relative importance of nucleation and growth
659 processes in -synuclein aggregation. *Proc. Natl. Acad. Sci.* **111:** 7671–7676 Available at:
660 http://www.pnas.org/cgi/doi/10.1073/pnas.1315346111

661 Burns RS, Chiueh CC, Markey SP, Ebert MH, Jacobowitz DM & Kopin IJ (1983) A primate
662 model of parkinsonism: selective destruction of dopaminergic neurons in the pars
663 compacta of the substantia nigra by N-methyl-4-phenyl-1,2,3,6-tetrahydropyridine.
664 *Proc. Natl. Acad. Sci.* **80:** 4546–4550 Available at:
665 http://www.pnas.org/cgi/doi/10.1073/pnas.80.14.4546

666 Campioni S, Carret G, Jordens S, Ce Nicoud L, Mezzenga R & Riek R (2014) The Presence of an
667 Air−Water Interface Affects Formation and Elongation of α‑Synuclein Fibrils.

668 Cenini G, Rub C, Bruderek M & Voos W (2016) Amyloid β-peptides interfere with
669 mitochondrial preprotein import competence by a coaggregation process. *Mol. Biol.*
670 *Cell* **27:** 3257–3272 Available at: http://www.molbiolcell.org/cgi/doi/10.1091/mbc.E16-
671 05-0313

672 Cha MY, Han SH, Son SM, Hong HS, Choi YJ, Byun J & Mook-Jung I (2012) Mitochondria-
673 specific accumulation of amyloid β induces mitochondrial dysfunction leading to
674 apoptotic cell death. *PLoS One* **7:**

675 Chan CS, Guzman JN, Ilijic E, Mercer JN, Rick C, Tkatch T, Meredith GE & Surmeier DJ (2007)
676 'Rejuvenation' protects neurons in mouse models of Parkinson's disease. *Nature* **447:**
677 1081–1086

678 Chan FTS, Schierle GSK, Kumita JR, Bertoncini CW, Dobson CM & Kaminski CF (2013) Protein
679 amyloids develop an intrinsic fluorescence signature during aggregation. *Analyst* **138:**
680 2156–2162

681 Chao YX, Ng EY, Foo JN, Liu J, Zhao Y & Tan EK (2015) Mitochondrial serine protease HTRA2
682 gene mutation in Asians with coexistent essential tremor and Parkinson disease.
683 *Neurogenetics* **16:** 241–242

de Chaumont F, Dallongeville S, Chenouard N, Hervé N, Pop S, Provoost T, Meas-Yedid V, Pankajakshan P, Lecomte T, Le Montagner Y, Lagache T, Dufour A & Olivo-Marin J-C (2012) Icy: an open bioimage informatics platform for extended reproducible research. *Nat. Methods* **9:** 690–696 Available at: http://www.nature.com/doifinder/10.1038/nmeth.2075

Chen W, Young LJ, Lu M, Zaccone A, Strohl F, Yu N, Schierle GSK & Kaminski CF (2017) Fluorescence self-quenching from reporter dyes informs on the structural properties of amyloid clusters formed in vitro and in cells. *Nano Lett.* **17:** 143–149

Chen WY, Avezov E, Schlachter SC, Gielen F, Laine RF, Harding HP, Hollfelder F, Ron D & Kaminski CF (2015) A method to quantify FRET stoichiometry with phasor plot analysis and acceptor lifetime ingrowth. *Biophys. J.* **108:** 999–1002 Available at: http://dx.doi.org/10.1016/j.bpj.2015.01.012

Chung SY, Kishinevsky S, Mazzulli JR, Graziotto J, Mrejeru A, Mosharov E V., Puspita L, Valiulahi P, Sulzer D, Milner TA, Taldone T, Krainc D, Studer L & Shim J won (2016) Parkin and PINK1 Patient iPSC-Derived Midbrain Dopamine Neurons Exhibit Mitochondrial Dysfunction and α-Synuclein Accumulation. *Stem Cell Reports* **7:** 664–677 Available at: http://dx.doi.org/10.1016/j.stemcr.2016.08.012

Cilenti L, Lee Y, Hess S, Srinivasula S, Park KM, Junqueira D, Davis H, Bonventre J V., Alnemri ES & Zervos AS (2003) Characterization of a novel and specific inhibitor for the pro-apoptotic protease Omi/HtrA2. *J. Biol. Chem.* **278:** 11489–11494

Criddle DN, Gillies S, Baumgartner-Wilson HK, Jaffar M, Chinje EC, Passmore S, Chvanov M, Barrow S, Gerasimenko O V., Tepikin A V., Sutton R & Petersen OH (2006) Menadione-induced reactive oxygen species generation via redox cycling promotes apoptosis of

murine pancreatic acinar cells. *J. Biol. Chem.* **281:** 40485–40492

Da Cruz LN, Alves E, Leal MT, Juliano MA, Rosenthal PJ, Juliano L & Garcia CRS (2011) FRET peptides reveal differential proteolytic activation in intraerythrocytic stages of the malaria parasites Plasmodium berghei and Plasmodium yoelii. *Int. J. Parasitol.* **41:** 363–372 Available at: http://dx.doi.org/10.1016/j.ijpara.2010.10.009

Dabir D V., Hasson SA, Setoguchi K, Johnson ME, Wongkongkathep P, Douglas CJ, Zimmerman J, Damoiseaux R, Teitell MA & Koehler CM (2013) A small molecule inhibitor of redox-regulated protein translocation into mitochondria. *Dev. Cell* **25:** 81–92 Available at: http://dx.doi.org/10.1016/j.devcel.2013.03.006

Demartino GN, Croall DE & Calcium-dependent DE (1982) Calcium-Dependent Proteases in Neuroblastoma Cells.

Devi L, Raghavendran V, Prabhu BM, Avadhani NG & Anandatheerthavarada HK (2008) Mitochondrial import and accumulation of α-synuclein impair complex I in human dopaminergic neuronal cultures and Parkinson disease brain. *J. Biol. Chem.* **283:** 9089–9100

Dull T, Zufferey R, Kelly M, Mandel RJ, Nguyen M, Trono D & Naldini L (1998) A third-generation lentivirus vector with a conditional packaging system. *J. Virol.* **72:** 8463–71 Available at: http://www.ncbi.nlm.nih.gov/pubmed/9765382%5Cnhttp://www.pubmedcentral.nih.gov/articlerender.fcgi?artid=PMC110254

Edelstein AD, Tsuchida MA, Amodaj N, Pinkard H, Vale RD & Stuurman N (2014) Advanced methods of microscope control using μManager software. *J. Biol. Methods* **1:** 10 Available at: http://www.jbmethods.org/jbm/article/view/36

730 Follett J, Darlow B, Wong MB, Goodwin J & Pountney DL (2013) Potassium depolarization
731 and raised calcium induces α-synuclein aggregates. *Neurotox. Res.* **23:** 378–92 Available
732 at: http://www.ncbi.nlm.nih.gov/pubmed/23250862

733 Friedman JR, Lackner LL, West M, DiBenedetto JR, Nunnari J & Voeltz GK (2011) ER Tubules
734 Mark Sites of Mitochondrial Division. *Science (80-.).* **334:** 358–362 Available at:
735 http://www.sciencemag.org/cgi/doi/10.1126/science.1207385

736 Gibellini L, Pinti M, Bartolomeo R, De Biasi S, Cormio A, Musicco C, Carnevale G, Pecorini S,
737 Nasi M, De Pol A & Cossarizza A (2015) Inhibition of Lon protease by triterpenoids alters
738 mitochondria and is associated to cell death in human cancer cells. *Oncotarget* **6:**
739 25466–83 Available at: http://www.ncbi.nlm.nih.gov/pubmed/26314956

740 Görlitz F, Kelly DJ, Warren SC, Alibhai D, West L, Kumar S, Alexandrov Y, Munro I, Garcia E,
741 McGinty J, Talbot C, Serwa RA, Thinon E, da Paola V, Murray EJ, Stuhmeier F, Neil MAA,
742 Tate EW, Dunsby C & French PMW (2017) Open Source High Content Analysis Utilizing
743 Automated Fluorescence Lifetime Imaging Microscopy. *J. Vis. Exp.***:** 1–11 Available at:
744 http://www.jove.com/video/55119/open-source-high-content-analysis-utilizing-
745 automated-fluorescence

746 Gottschalk WK, Lutz MW, He YT, Saunders AM, Daniel K, Roses AD, Chiba-falek O & Hill C
747 (2014) The Broad Impact of TOM40 on Neurodegenerative Diseases in Aging. *J Park. Dis*
748 *Alzheimers Dis* **1:** 1–25

749 Gray CW, Ward R V., Karran E, Turconi S, Rowles A, Viglienghi D, Southan C, Barton A,
750 Fantom KG, West A, Savopoulos J, Hassan NJ, Clinkenbeard H, Hanning C, Amegadzie B,
751 Davis JB, Dingwall C, Livi GP & Creasy CL (2000) Characterization of human HtrA2, a
752 novel serine protease involved in the mammalian cellular stress response. *Eur. J.*

Biochem. **267:** 5699–5710

Greenamyre JT, Sherer TB, Betarbet R & Panov a V (2001) Complex I and Parkinson's disease. *IUBMB Life* **52:** 135–141

Gupta S, Singh R, Datta P, Zhang ZJ, Orr C, Lu Z, DuBois G, Zervos AS, Meisler MH, Srinivasula SM, Fernandes-Alnemri T & Alnemri ES (2004) The C-terminal tail of presenilin regulates Omi/HtrA2 protease activity. *J. Biol. Chem.* **279:** 45844–45854

Gur E & Sauer RT (2008) Recognition of misfolded proteins by Lon, a AAA+ protease. *Genes Dev.* **22:** 2267–2277

Herbert S, Ortmann W, Lautenschl J, Marco K, Grosskreutz J & Denzler J (2014) Quantitative Analysis of Pathological Mitochondrial Morphology in Neuronal Cells in Confocal Laser Scanning Microscopy Images. *Proc. IWBBIO***:** 1290–1301

Huang C, Ren G, Zhou H & Wang C (2005) A new method for purification of recombinant human alpha-synuclein in Escherichia coli. *Protein Expr. Purif.* **42:** 173–177

Imamura H, Nhat KPH, Togawa H, Saito K, Iino R, Kato-Yamada Y, Nagai T & Noji H (2009) Visualization of ATP levels inside single living cells with fluorescence resonance energy transfer-based genetically encoded indicators. *Proc. Natl. Acad. Sci. U. S. A.* **106:** 15651–15656

Jones JM, Datta P, Srinivasula SM, Ji W, Gupta S, Zhang ZJ, Davies E, Hajnóczky G, Saunders TL, Van Keuren ML, Fernandes-Alnemri T, Meisler MH & Alnemri ES (2003) Loss of Omi mitochondrial protease activity causes the neuromuscular disorder of mnd2 mutant mice. *Nature* **425:** 721–727

Kaminski Schierle GS, Bertoncini CW, Chan FTS, Van Der Goot AT, Schwedler S, Skepper J, Schlachter S, Van Ham T, Esposito A, Kumita JR, Nollen EAA, Dobson CM & Kaminski CF

(2011) A FRET sensor for non-invasive imaging of amyloid formation in vivo. *ChemPhysChem* **12:** 673–680

Kawamoto Y, Kobayashi Y, Suzuki Y, Inoue H, Tomimoto H, Akiguchi I, Budka H, Martins LM, Downward J & Takahashi R (2008) Accumulation of HtrA2/Omi in neuronal and glial inclusions in brains with α-synucleinopathies. *J. Neuropathol. Exp. Neurol.* **67:** 984–993

Kordower JH & Brundin P (2009) Lewy body pathology in long-term fetal nigral transplants: Is Parkinson's disease transmitted from one neural system to another? *Neuropsychopharmacology* **34:** 254

Kotera I, Iwasaki T, Imamura H, Noji H & Nagai T (2010) Reversible Dimerization of Aequorea victoria Fluorescent Proteins Increases the Dynamic Range of FRET-Based Indicators. *ACS Chem. Biol.* **5:** 321–332

Langston J, Ballard P, Tetrud J & Irwin I (1983) Chronic Parkinsonism in humans due to a product of meperidine-analog synthesis. *Science (80-.).* **219:** 979–980 Available at: http://www.sciencemag.org/cgi/doi/10.1126/science.6823561

Lautenschläger J, Lautenschläger C, Tadic V, S????e H, Ortmann W, Denzler J, Stallmach A, Witte OW & Grosskreutz J (2015) Novel computer vision algorithm for the reliable analysis of organelle morphology in whole cell 3D images - A pilot study for the quantitative evaluation of mitochondrial fragmentation in amyotrophic lateral sclerosis. *Mitochondrion* **25:** 49–59 Available at: http://dx.doi.org/10.1016/j.mito.2015.10.003

Lautenschläger J, Stephens AD, Fusco G, Ströhl F, Curry N, Zacharopoulou M, Michel CH, Laine R, Nespovitaya N, Fantham M, Pinotsi D, Zago W, Fraser P, Tandon A, St George-Hyslop P, Rees E, Phillips JJ, De Simone A, Kaminski CF & Schierle GSK (2018) C-terminal calcium binding of α-synuclein modulates synaptic vesicle interaction. *Nat. Commun.* **9:**

712 Available at: http://www.nature.com/articles/s41467-018-03111-4

Lee BR & Kamitani T (2011) Improved immunodetection of endogenous α-synuclein. *PLoS One* **6:**

Liu ML, Liu MJ, Kim JM, Kim HJ, Kim JH & Hong ST (2005) HtrA2 interacts with A beta peptide but does not directly alter its production or degradation. *Mol Cells* **20:** 83–89 Available at: http://www.ncbi.nlm.nih.gov/pubmed/16258245

Lu M, Williamson N, Mishra A, Michel CH, Kaminski CF, Tunnacliffe A & Kaminski Schierle GS (2019) Structural progression of amyloid- Arctic mutant aggregation in cells revealed by multiparametric imaging. *J. Biol. Chem.* **294:** 1478–1487

Lu X-H, Fleming SM, Meurers B, Ackerson LC, Mortazavi F, Lo V, Hernandez D, Sulzer D, Jackson GR, Maidment NT, Chesselet M-F & Yang XW (2009) Bacterial Artificial Chromosome Transgenic Mice Expressing a Truncated Mutant Parkin Exhibit Age-Dependent Hypokinetic Motor Deficits, Dopaminergic Neuron Degeneration, and Accumulation of Proteinase K-Resistant -Synuclein. *J. Neurosci.* **29:** 1962–1976 Available at: http://www.jneurosci.org/cgi/doi/10.1523/JNEUROSCI.5351-08.2009

Ludtmann MHR, Angelova PR, Ninkina NN, Gandhi S, Buchman VL & Abramov AY (2016) Monomeric Alpha-Synuclein Exerts a Physiological Role on Brain ATP Synthase. *J. Neurosci.* **36:** 10510–10521 Available at: http://www.ncbi.nlm.nih.gov/pubmed/27733604%5Cnhttp://www.ncbi.nlm.nih.gov/pubmed/27733604

Luk KC, Kehm VM, Zhang B, O'Brien P, Trojanowski JQ & Lee VMY (2012) Intracerebral inoculation of pathological α-synuclein initiates a rapidly progressive neurodegenerative α-synucleinopathy in mice. *J. Exp. Med.* **209:** 975–86 Available at:

http://jem.rupress.org/content/209/5/975.long

Luk KC, Song C, O'Brien P, Stieber A, Branch JR, Brunden KR, Trojanowski JQ & Lee VM-Y (2009) Exogenous alpha-synuclein fibrils seed the formation of Lewy body-like intracellular inclusions in cultured cells. *Proc. Natl. Acad. Sci. U. S. A.* **106:** 20051–6 Available at: http://www.pnas.org/content/106/47/20051.full

Di Maio R, Barrett PJ, Hoffman EK, Barrett CW, Zharikov A, Borah A, Hu X, McCoy J, Chu CT, Burton EA, Hastings TG & Greenamyre JT (2016) α-synuclein binds to TOM20 and inhibits mitochondrial protein import in Parkinson's disease. *Sci. Transl. Med.* **8:** 1–14

Marchenko S & Flanagan L (2007) Immunocytochemistry: human neural stem cells. *J. Vis. Exp.***:** 267

Martínez JH, Fuentes F, Vanasco V, Alvarez S, Cassina A, Leskow FC & Velazquez F (2018) Mitochondrial interaction of alpha-synuclein leads to irreversible translocation and complex I impairment. *Arch. Biochem. Biophys.* **651:** 1–12 Available at: https://doi.org/10.1016/j.abb.2018.04.018

Martins LM, Morrison A, Klupsch K, Fedele V, Moisoi N, Teismann P, Abuin A, Grau E, Geppert M, George P, Creasy CL, Martin A, Hargreaves I, Heales SJ, Okada H, Brandner S, Schulz B, Mak T, Downward J & Livi GP (2004) Neuroprotective Role of the Reaper-Related Serine Protease HtrA2 / Omi Revealed by Targeted Deletion in Mice. *Mol. Cell. Biol.* **24:** 9848–9862

Mellgren L (1987) Calcium-dependent proteases: an enzyme system active at cellular membranes? *FASEB J* **1:** 110–5

Mossmann D, Vögtle FN, Taskin AA, Teixeira PF, Ring J, Burkhart JM, Burger N, Pinho CM, Tadic J, Loreth D, Graff C, Metzger F, Sickmann A, Kretz O, Wiedemann N, Zahedi RP,

845 Madeo F, Glaser E & Meisinger C (2014) Amyloid-β peptide induces mitochondrial
846 dysfunction by inhibition of preprotein maturation. *Cell Metab.* **20:** 662–669

847 Müller M, Mönkemöller V, Hennig S, Hübner W & Huser T (2016) Open-source image
848 reconstruction of super-resolution structured illumination microscopy data in ImageJ.
849 *Nat. Commun.* **7:** 1–6

850 Nath S, Goodwin J, Engelborghs Y & Pountney DL (2011) Raised calcium promotes α-
851 synuclein aggregate formation. *Mol. Cell. Neurosci.* **46:** 516–526 Available at:
852 http://linkinghub.elsevier.com/retrieve/pii/S1044743110002678

853 Park HJ, Seong YM, Choi JY, Kang S & Rhim H (2004) Alzheimer's disease-associated amyloid
854 beta interacts with the human serine protease HtrA2/Omi. *Neurosci. Lett.* **357:** 63–67

855 Peelaerts W, Bousset L, Van Der Perren A, Moskalyuk A, Pulizzi R, Giugliano M, Van Den
856 Haute C, Melki R & Baekelandt V (2015) α-Synuclein strains cause distinct
857 synucleinopathies after local and systemic administration. *Nature* **522:** 340–344

858 Pinotsi D, Michel CH, Buell AK, Laine RF, Mahou P, Dobson CM, Kaminski CF & Kaminski GS
859 (2016) Nanoscopic insights into seeding mechanisms and toxicity of α -synuclein species
860 in neurons. *PNAS* **113:** 3815–3819

861 Plun-Favreau H, Klupsch K, Moisoi N, Gandhi S, Kjaer S, Frith D, Harvey K, Deas E, Harvey RJ,
862 McDonald N, Wood NW, Martins LM & Downward J (2007) The mitochondrial protease
863 HtrA2 is regulated by Parkinson's disease-associated kinase PINK1. *Nat. Cell Biol.* **9:**
864 1243–1252 Available at: http://www.nature.com/doifinder/10.1038/ncb1644

865 Quirós PM, Langer T & López-Otín C (2015) New roles for mitochondrial proteases in health,
866 ageing and disease. *Nat. Rev. Mol. Cell Biol.* **16:** 345–359 Available at:
867 http://www.nature.com/doifinder/10.1038/nrm3984

868 Ray P, Chakrabarti AK, Broomfield CA & Ray R (2002) Sulfur mustard-stimulated protease: A
869 target for antivesicant drugs. *J. Appl. Toxicol.* **22:** 139–140

870 Reeve a K, Ludtmann MH, Angelova PR, Simcox EM, Horrocks MH, Klenerman D, Gandhi S,
871 Turnbull DM & Abramov a Y (2015) Aggregated α-synuclein and complex I deficiency:
872 exploration of their relationship in differentiated neurons. *Cell Death Dis.* **6:** e1820
873 Available at: http://www.ncbi.nlm.nih.gov/pubmed/26181201

874 Robotta M, Gerding HR, Vogel A, Hauser K, Schildknecht S, Karreman C, Leist M,
875 Subramaniam V & Drescher M (2014) Alpha-synuclein binds to the inner membrane of
876 mitochondria in an a-helical conformation. *ChemBioChem* **15:** 2499–2502

877 Ruan L, Zhou C, Jin E, Kucharavy A, Zhang Y, Wen Z, Florens L & Li R (2017) Cytosolic
878 proteostasis through importing of misfolded proteins into mitochondria. *Nature* **543:**
879 443–446 Available at: http://www.nature.com/doifinder/10.1038/nature21695

880 Rui Y & Zheng JQ (2016) Amyloid β oligomers elicit mitochondrial transport defects and
881 fragmentation in a time-dependent and pathway-specific manner. *Mol. Brain* **9:** 79
882 Available at:
883 http://www.ncbi.nlm.nih.gov/pubmed/27535553%5Cnhttp://www.pubmedcentral.nih.
884 gov/articlerender.fcgi?artid=PMC4989350

885 Ryan T, Bamm V V., Stykel MG, Coackley CL, Humphries KM, Jamieson-Williams R,
886 Ambasudhan R, Mosser DD, Lipton SA, Harauz G & Ryan SD (2018) Cardiolipin exposure
887 on the outer mitochondrial membrane modulates α-synuclein. *Nat. Commun.* **9:** 1–17
888 Available at: http://dx.doi.org/10.1038/s41467-018-03241-9

889 Sancak Y, Peterson TR, Shaul YD, Lindquist RA, Thoreen CC, Bar-Peled L & Sabatini DM (2008)
890 The rag GTPases bind raptor and mediate amino acid signaling to mTORC1. *Science (80-.*

). **320:** 1496–1501

Schierle GSK, Sauer M & Kaminski CF (2014) Probing Amyloid Aggregation and Morphology In Situ by Multiparameter Imaging and Super-Resolution Fluorescence Microscopy. *Bio-nanoimaging***:** 105–120

Schindelin J, Arganda-Carreras I, Frise E, Kaynig V, Longair M, Pietzsch T, Preibisch S, Rueden C, Saalfeld S, Schmid B, Tinevez J-Y, White DJ, Hartenstein V, Eliceiri K, Tomancak P & Cardona A (2012) Fiji: an open-source platform for biological-image analysis. *Nat. Methods* **9:** 676–682 Available at: http://www.nature.com/doifinder/10.1038/nmeth.2019

Sherer TB, Kim J-H, Betarbet R & Greenamyre JT (2003) Subcutaneous Rotenone Exposure Causes Highly Selective Dopaminergic Degeneration and α-Synuclein Aggregation. *Exp. Neurol.* **179:** 9–16 Available at: http://www.sciencedirect.com/science/article/pii/S001448602980726%5Cnhttp://www.sciencedirect.com/science/article/pii/S0014488602980726/pdf?md5=2eab2f018db2b1d971489608006acdcb&pid=1-s2.0-S0014488602980726-main.pdf

Sorrentino V, Romani M, Mouchiroud L, Beck JS, Zhang H, D'Amico D, Moullan N, Potenza F, Schmid AW, Rietsch S, Counts SE & Auwerx J (2017) Enhancing mitochondrial proteostasis reduces amyloid-β proteotoxicity. *Nature* **552:** 187–193 Available at: http://www.nature.com/doifinder/10.1038/nature25143

Stopschinski BE & Diamond MI (2017) The prion model for progression and diversity of neurodegenerative diseases. *Lancet Neurol.* **16:** 323–332 Available at: http://dx.doi.org/10.1016/S1474-4422(17)30037-6

Strauss KM, Martins LM, Plun-Favreau H, Marx FP, Kautzmann S, Berg D, Gasser T, Wszolek

914 Z, Müller T, Bornemann A, Wolburg H, Downward J, Riess O, Schulz JB & Krüger R (2005)
915 Loss of function mutations in the gene encoding Omi/HtrA2 in Parkinson's disease.
916 *Hum. Mol. Genet.* **14:** 2099–2111

917 Subramaniam SR, Vergnes L, Franich NR, Reue K & Chesselet MF (2014) Region specific
918 mitochondrial impairment in mice with widespread overexpression of alpha-synuclein.
919 *Neurobiol. Dis.* **70:** 204–213 Available at: http://dx.doi.org/10.1016/j.nbd.2014.06.017

920 Sum TH, Sum TJ, Galloway WRJD, Collins S, Twigg DG, Hollfelder F & Spring DR (2016)
921 Combinatorial synthesis of structurally diverse triazole-bridged flavonoid dimers and
922 trimers. *Molecules* **21:**

923 Thakur P, Breger LS, Lundblad M, Wan OW, Mattsson B, Luk KC, Lee VMY, Trojanowski JQ &
924 Björklund A (2017) Modeling Parkinson's disease pathology by combination of fibril
925 seeds and α-synuclein overexpression in the rat brain. *Proc. Natl. Acad. Sci.***:** 201710442
926 Available at: http://www.pnas.org/lookup/doi/10.1073/pnas.1710442114

927 Unal Gulsuner H, Gulsuner S, Mercan FN, Onat OE, Walsh T, Shahin H, Lee MK, Dogu O,
928 Kansu T, Topaloglu H, Elibol B, Akbostanci C, King M-C, Ozcelik T & Tekinay AB (2014)
929 Mitochondrial serine protease HTRA2 p.G399S in a kindred with essential tremor and
930 Parkinson disease. *Proc. Natl. Acad. Sci.* **111:** 18285–18290 Available at:
931 http://www.pnas.org/lookup/doi/10.1073/pnas.1419581111

932 Vaux DL & Silke J (2003) HtrA2/Omi, a sheep in Wolf's clothing. *Cell* **115:** 251–253

933 Wang LF, Christensen BN, Bhatnagar A & Srivastava SK (2001) Role of calcium-dependent
934 protease(s) in globulization of isolated rat lens cortical fiber cells. *Investig. Ophthalmol.*
935 *Vis. Sci.* **42:** 194–199

936 Warren SC, Margineanu A, Alibhai D, Kelly DJ, Talbot C, Alexandrov Y, Munro I, Katan M,

937 Dunsby C & French PMW (2013) Rapid Global Fitting of Large Fluorescence Lifetime
938 Imaging Microscopy Datasets. *PLoS One* **8:**

939 Westerlund M, Behbahani H, Gellhaar S, Forsell C, Belin AC, Anvret A, Zettergren A,
940 Nissbrandt H, Lind C, Sydow O, Graff C, Olson L, Ankarcrona M & Galter D (2011)
941 Altered enzymatic activity and allele frequency of OMI/HTRA2 in Alzheimer's disease.
942 *FASEB J.* **25:** 1345–52 Available at: http://www.fasebj.org/cgi/doi/10.1096/fj.10-
943 163402%5Cnhttp://www.ncbi.nlm.nih.gov/pubmed/21163861%5Cnhttp://www.pubme
944 dcentral.nih.gov/articlerender.fcgi?artid=PMC3228343%5Cnhttp://www.pubmedcentra
945 l.nih.gov/articlerender.fcgi?artid=3228343&tool=pmcentrez&r

946 Wu H, Zhang F, Williamson N, Jian J, Zhang L, Liang Z, Wang J, An L, Tunnacliffe A & Zheng Y
947 (2014) Effects of secondary metabolite extract from Phomopsis occultaon β-amyloid
948 aggregation. *PLoS One* **9:**

949 Young LJ, Ströhl F & Kaminski CF (2016) A Guide to Structured Illumination TIRF Microscopy
950 at High Speed with Multiple Colors. *J. Vis. Exp.*: 1–16 Available at:
951 http://www.jove.com/video/53988/a-guide-to-structured-illumination-tirf-microscopy-
952 at-high-speed-with

953

954

955

956

957

958

959

960 **Figure Legends**

961

962 **Fig. 1. The preformed fibril (PFF) model mimics alpha-synuclein seeding in disease.**

963 (A) Schematic overview of the PFF assay.

964 (B) Structured illumination microscopy (SIM) images of SH-SY5Y cells overexpressing YFP-
965 tagged alpha-synuclein without alpha-synuclein fibrillization (left) and upon PFF-induced
966 seeding (right). Scale bars: 10 µm.

967 (C and D) Co-staining of YFP-alpha-synuclein fibrils with ubiquitin and ubiquitin-binding
968 protein p62. Scale bars: 10 µm.

969

970 **Fig. 2. Mitochondrial dysfunction increases alpha-synuclein seeding.**

971 (A) YFP-alpha-synuclein SH-SY5Y cells treated with DMSO (control), 10 µM BAPTA-AM before
972 (1h) or before and during the incubation with PFFs (5h). Scale bars: 20 µm. Alpha-synuclein
973 seeding was increased upon 1h pre-treatment and 5h treatment with BAPTA-AM. Data are
974 presented as mean ± SEM. *p = 0.0127 and ****p < 0.0001 (Kruskal-Wallis test with Dunn's
975 multiple comparison). N = 16, 9, 15 with n = regions analyzed, three biological repeats.

976 (B) FLIM measurements of cytosolic calcium in SH-SY5Y cells treated with DMSO (control) or
977 10 µM BAPTA-AM for 10 min, 1h or 5h. The cytosolic calcium level was significantly reduced
978 upon 10 min incubation with BAPTA-AM, however after 1h calcium returned to basal levels,
979 reaching significantly increased concentrations after 5h treatment. Data are presented as
980 mean ± SEM. ****p < 0.0001 (Kruskal-Wallis test with Dunn's multiple comparison). N = 88,
981 54, 61, 46, with n = cells analyzed, three biological repeats.

982 (C) ThT assay of in vitro alpha-synuclein aggregation in the presence of DMSO, 10 µM BAPTA-
983 AM, or 10 µM BAPTA. Data from three biological repeats.

(D) SIM images of mitochondrial network stained with Mito-RFP in SH-SH5Y cells treated with DMSO (control) or 10 µM BAPTA-AM. Scale bars: 5 µm.

(E) YFP-alpha-synuclein SH-SY5Y cells treated with DMSO (control), 10 µM FCCP before (1h) or before and during the incubation with PFFs (5h). Scale bars: 20 µm. Alpha-synuclein seeding was increased upon 5h treatment with FCCP. Data are presented as mean ± SEM. **p = 0.0064 (Kruskal-Wallis test with Dunn's multiple comparison). N = 16, 6, 9 with n = regions analyzed, three biological repeats.

(F) ThT assay of in vitro alpha-synuclein aggregation in the presence of DMSO or 10 µM FCCP. Data from three biological repeats.

Fig. 3. Downstream effectors of mitochondrial dysfunction do not influence alpha-synuclein seeding.

(A) YFP-alpha-synuclein SH-SY5Y cells treated with DMSO (control), 500 µM MPP^+, 1 µM ionomycin, or 3 µM menadione for 3 days (1h before, during PFF incubation, and during seeding). Scale bars: 20 µm. Alpha-synuclein seeding was not significantly increased (one-way ANOVA with Dunnett's post-hoc correction). Data are presented as mean ± SEM, N = 11, 8, 8, 7 with n = regions analyzed, three biological repeats.

(B) FLIM measurements of ATP levels, cytosolic calcium, and H_2O_2 in SH-SY5Y cells treated with DMSO (control), the respective positive control, 10 µM FCCP and 10 µM BAPTA-AM for 1 h. Scale bars: 20 µm.

(C) The effect of 500 µM MPP^+ on ATP levels was lower than with FCCP, but higher than the effect of BAPTA-AM. The effect of 1 µM ionomycin on cytosolic calcium levels was higher than with FCCP and BAPTA-AM. The effect of 3 µM menadione on cytosolic H_2O_2 levels was comparable with the effect of FCCP and BAPTA-AM. Data are presented as mean ± SEM. ****p

< 0.0001 and N = 43, 74, 48, 47 for ATP levels. ****p < 0.0001 and N = 88, 60, 42, 61 for cytosolic calcium levels. **p = 0.0017, p = 0.0012 and p = 0.0058 and N = 79, 63, 36, 70 for cytosolic H_2O_2 levels (Kruskal-Wallis test with Dunn's multiple comparison), with n = cells analyzed, three biological repeats.

(D and E) Quantification of mitochondrial fragmentation for 5h treatments, showing significant reduced mitochondrial length upon treatment with FCCP and BAPTA-AM. Data are presented as mean ± SEM. ****p < 0.0001 (Kruskal-Wallis test with Dunn's multiple comparison). N = 76, 92, 103, 90, 88, 89 with n = individual images, three biological repeats. Images analysis for mitochondria fragmentation using NIEL Mito (Lautenschläger *et al*, 2015), scale bars: 10 µm.

Fig. 4. Inhibition of mitochondrial proteases and mitochondrial protein import increase alpha-synuclein seeding.

(A) YFP-alpha-synuclein SH-SY5Y cells treated with DMSO (control), 1 µM CDDO-Me, or 20 µM UCF-101 before and during the incubation with PFFs (5h). Scale bars: 20 µm. Alpha-synuclein seeding was increased upon both treatments. Data are presented as mean ± SEM. **p = 0.005 and ****p < 0.0001 (Kruskal-Wallis test with Dunn's multiple comparison). N = 15, 9, 11 with n = regions analyzed, three biological repeats.

(B) Western blot of mitochondria isolated from adult rat brain, native, proteinase K (PK) or PK in the presence of 0.1% TritonX-100.

(C) Relative intensity of bands normalized to native mitochondria. Data are presented as mean ± SEM. ***p = 0.0007, ****p = < 0.0001, **p = 0.0017 (one-way ANOVA with Tukey's post-hoc correction). N = 3 for all conditions with n = biological repeats.

(D) Transmission electron microscopy (TEM) of YFP alpha-synuclein SH-SY5Y cells showing that alpha-synuclein is contained within mitochondria. Arrows indicate individual immunogold labelling within mitochondria. m = mitochondria, cyt = cytoplasm. Scale bar: 100 nm.

(E) YFP-alpha-synuclein SH-SY5Y cells treated with DMSO (control), or 50 µM MitobloCK-6 before and during the incubation with PFFs (5h). Scale bars: 20 µm. Alpha-synuclein seeding was significantly increased upon treatment. Data are presented as mean ± SEM. ****p < 0.0001 (two-tailed Mann-Whitney U test). N = 15, 11 with n = regions analyzed, three biological repeats.

Fig. 5. Mitochondrial proteostasis influences β-amyloid 42 aggregation.

(A) Aβ42-mCherry cells treated with DMSO (control), 1 µM FCCP or 10 µM BAPTA-AM for 24 h. The aggregation of Aβ42 was increased upon treatment with FCCP and BAPTA-AM. Data are presented as mean ± SEM. *p = 0.0298 and ****p < 0.0001 (Kruskal-Wallis test with Dunn's multiple comparison). N = 9, for all conditions, with n = wells analyzed, three biological repeats.

(B) Aβ42-mCherry cells treated with DMSO (control), 0.1 µM CDDO-Me or 20 µM UCF-101 for 24 h. The aggregation of Aβ42 was increased upon treatment with UCF-101. Data are presented as mean ± SEM. ***p = 0.0001 (one-way ANOVA with Dunnett's post-hoc correction). N = 9, for all conditions, with n = wells analyzed, three biological repeats.

(C) Aβ42-mCherry cells treated with DMSO (control) or 5 µM MitobloCK-6 for 24 h. The aggregation of Aβ42 was increased upon treatment with MitobloCK-6. Data are presented as mean ± SEM. **p = 0.0088 (two-tailed unpaired t-test). N = 9, for all conditions, with n = wells analyzed, three biological repeats.

(D) Aβ42-mCherry cells were transfected with either uncut pcDNA3 (control) or HtrA2 pcDNA3 and Aβ42-mCherry expression was induced with tetracycline for 3 days. The aggregation of Aβ42 was decreased upon overexpression of HtrA2. Data are presented as mean ± SEM. **p = 0.0089 (two-tailed unpaired t-test). N = 9, 9 with n = regions analyzed, three biological repeats.

Scale bars: 20 µm.

Fig. 6. HtrA2 influences in-vitro aggregation of β-amyloid 42.

(A) FLIM measurements for the aggregation of Aβ42 at the beginning of the experiment (time 0) and after 2 hours of incubation at room temperature (time 2 hrs), showing a decrease in lifetime in control conditions demonstrating aggregation of the protein. No decrease in lifetime, i.e. aggregation was evident upon addition of isolated mitochondria. Data are presented as mean ± SEM. **p =0.0025 and ****p< 0.0001 (one-way ANOVA with Tukey's post-hoc correction). N = 7, 8, 7, 7 with n = wells analyzed, three biological repeats. Scale bars: 20 µm.

(B) FLIM measurements for the aggregation of Aβ42 at the beginning of the experiment (time 0) and after 2 hours of incubation at room temperature (time 2 hrs), showing a decrease in lifetime when UCF-101 treated mitochondria were added. Data are presented as mean ± SEM. ***p =0.0009 and *p= 0.0142 (one-way ANOVA with Tukey's post-hoc correction). N = 8, 8, 7, 8 with n = wells analyzed, three biological repeats. Scale bars: 20 µm.

FigEV. 1. AFM of preformed alpha-synuclein fibrils

Preformed fibrils generated from recombinant human wild-type alpha-synuclein shown by atomic force microscopy before (upper panel) and after sonication (lower panel). Scale bars: 1 µm.

FigEV. 2. Example images of immunogold TEM, supplementary to Fig. 4D

(A) Representative images of transmission electron microscopy (TEM) from SH-SY5Y cells overexpressing YFP-alpha-synuclein showing that alpha-synuclein is contained within mitochondria. Arrows indicate individual immunogold labelling within mitochondria. Scale bars: 500 nm.

(B) TEM images and quantification of anti-GFP staining in control SH-SY5Y cells and SH-SY5Y cells overexpressing YFP-alpha-synuclein. Data are presented as mean ± SEM. ***p = 0.0002 (two-tailed unpaired t-test). N = 10, 13 with n = images analyzed. Scale bars: 500 nm.

Figures

Figure 1

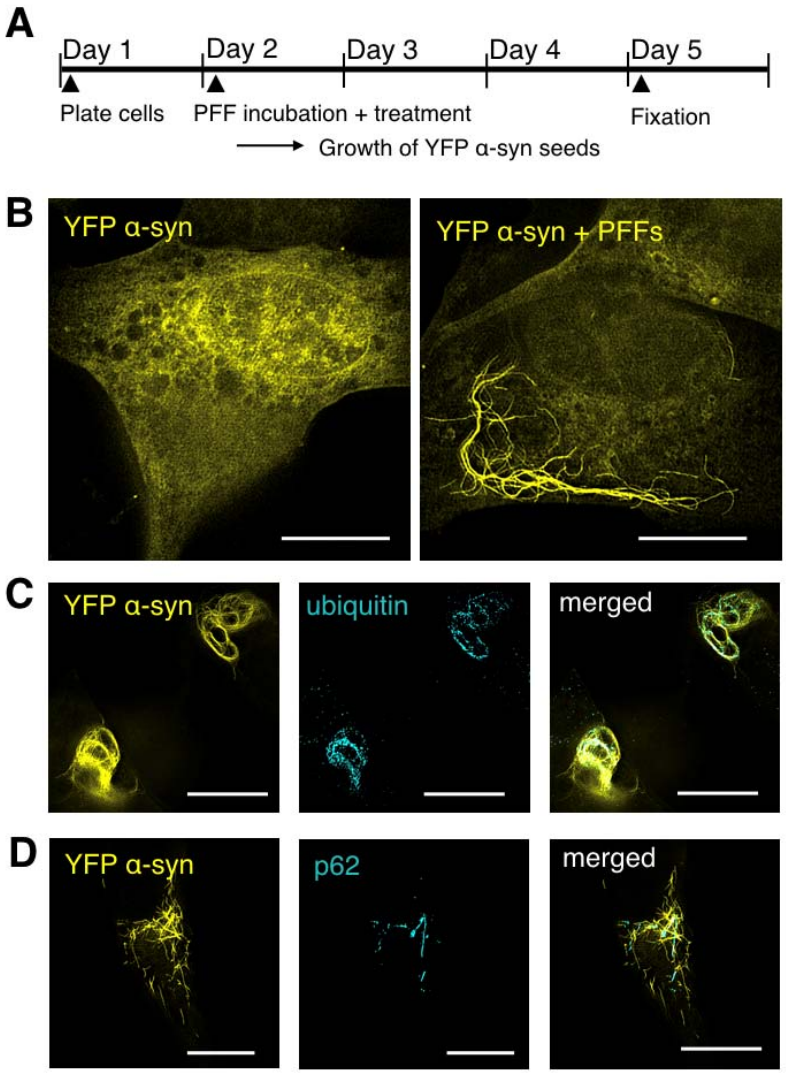

Figure 2

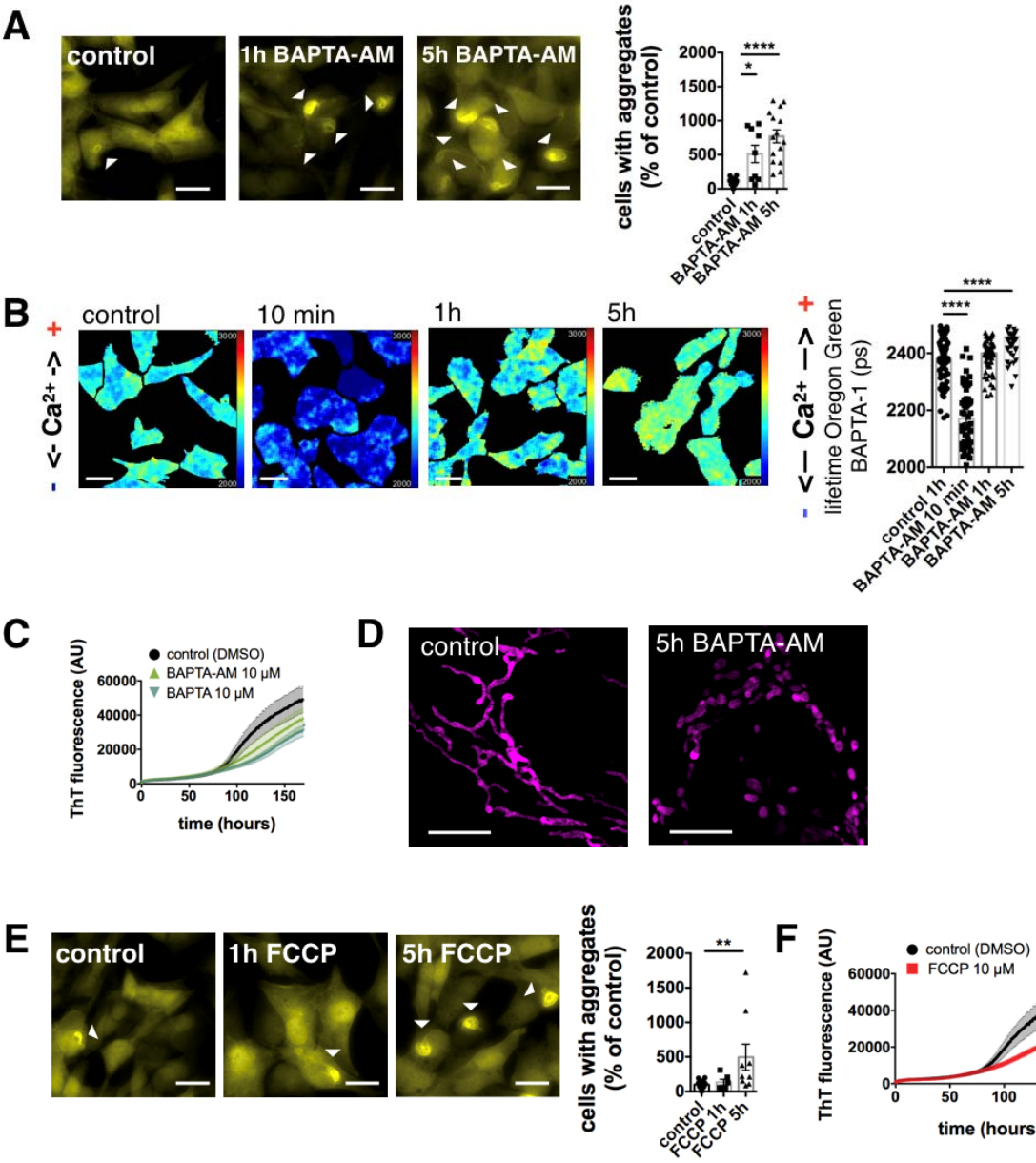

Figure 3

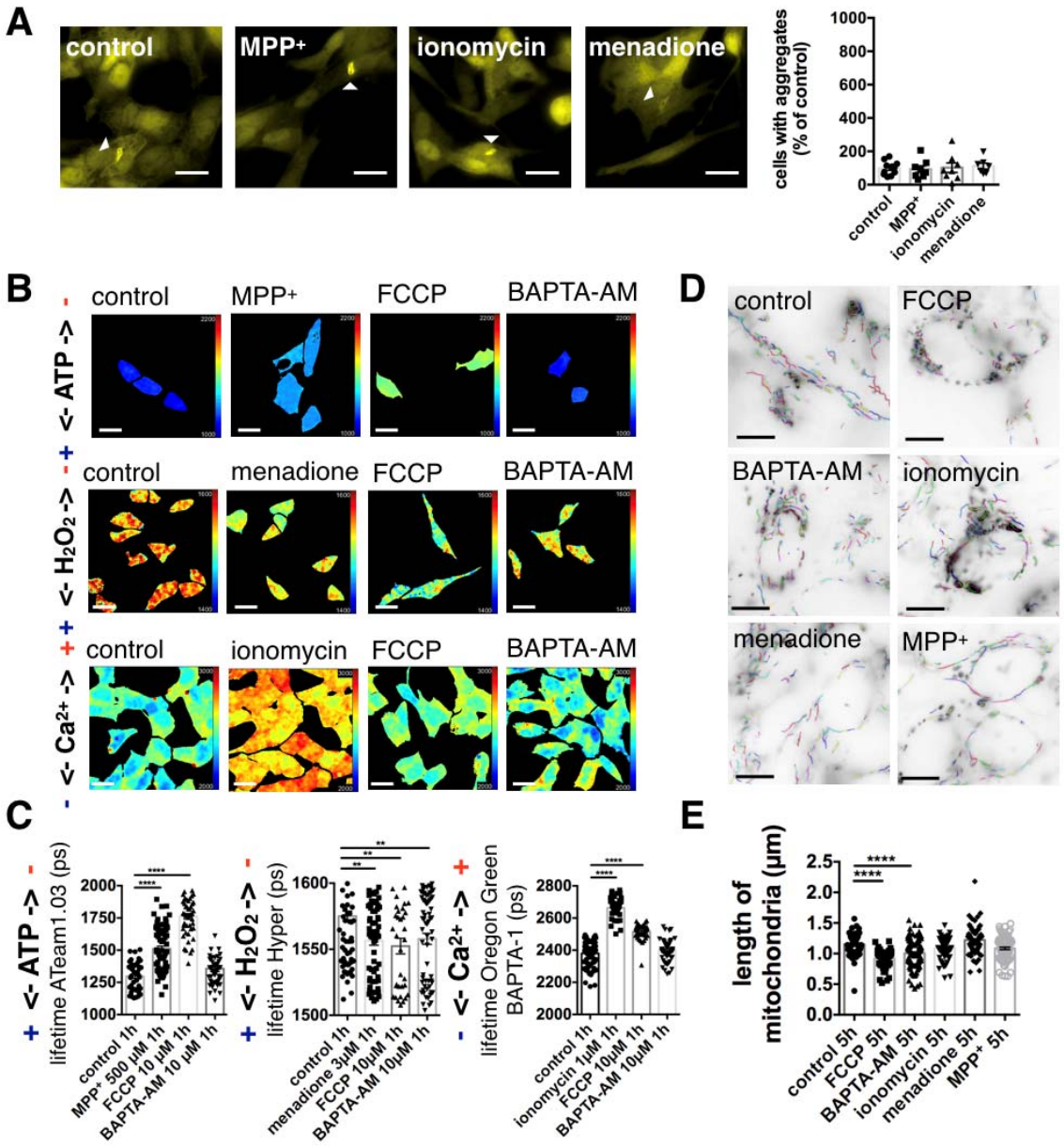

Figure 4

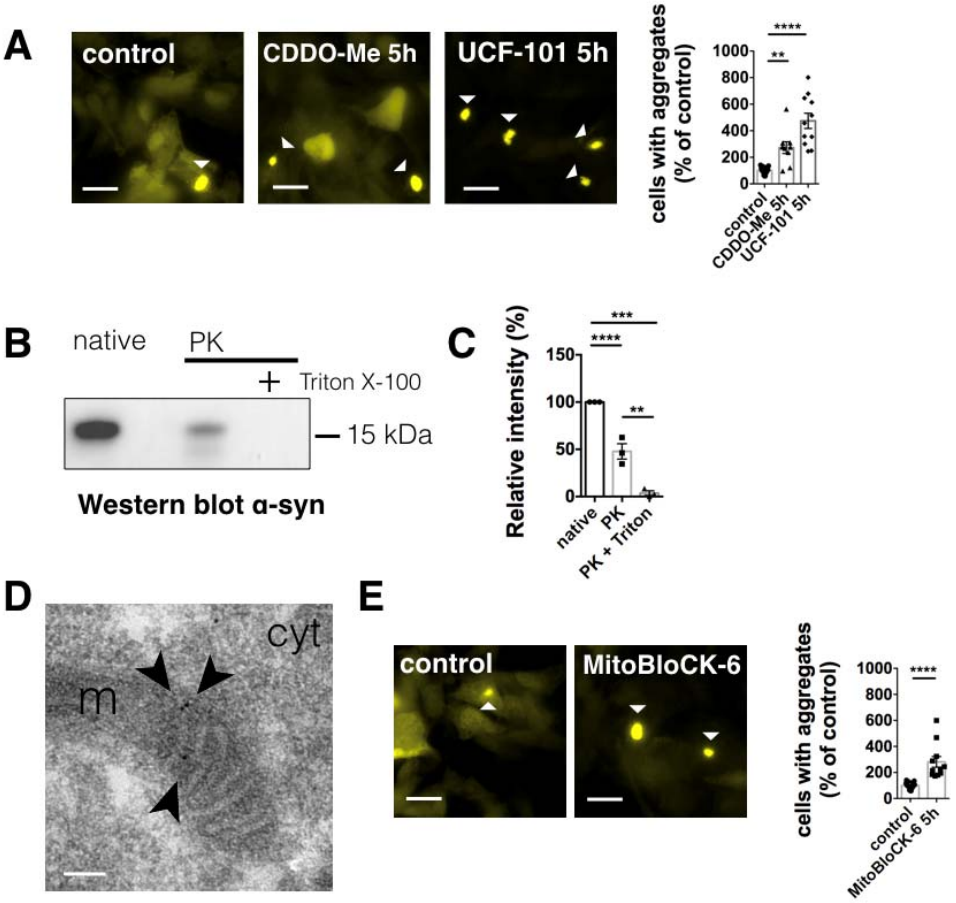

1143 **Figure 5**

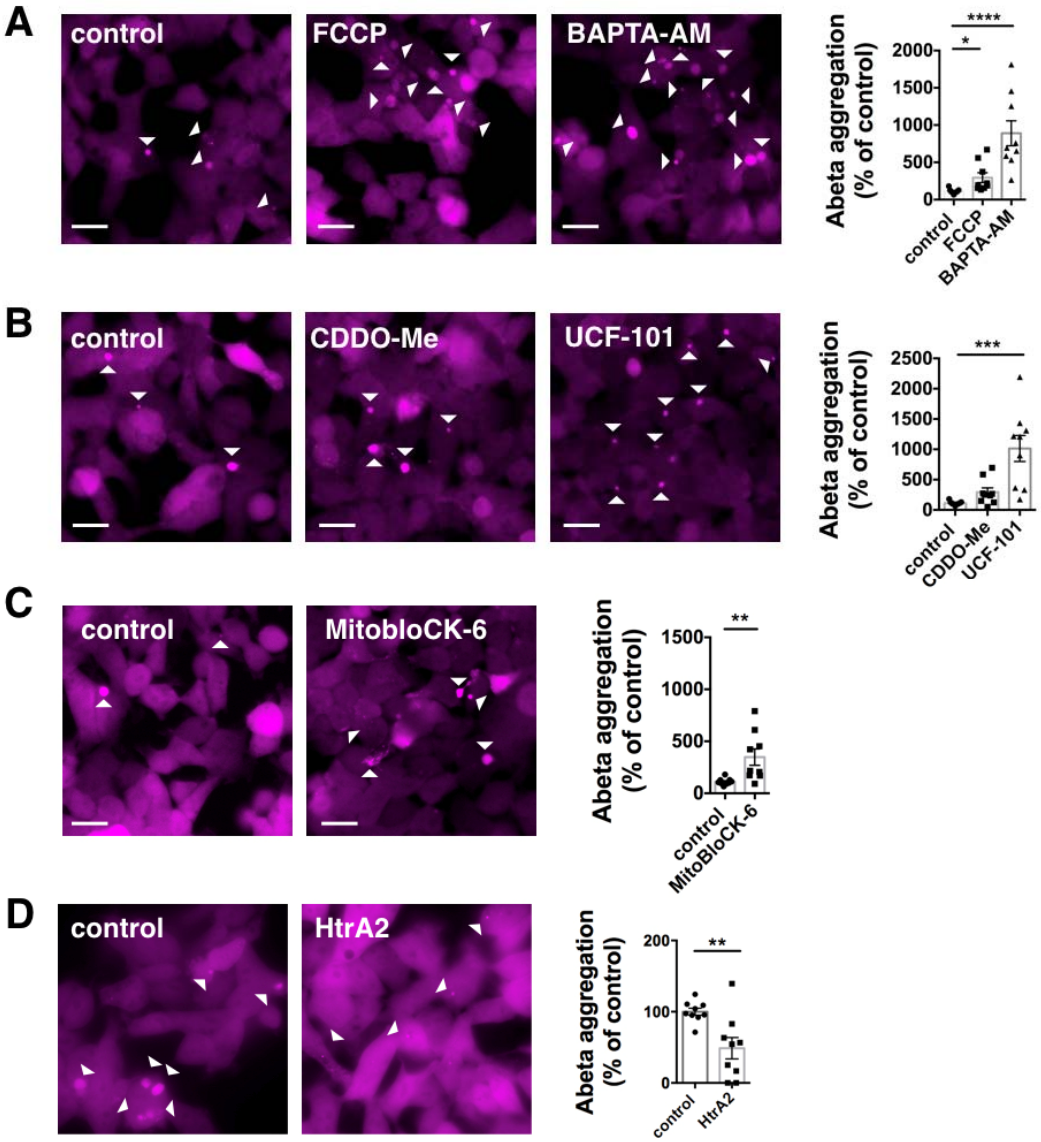

1144

1145

1146

1147

1148

1149

1150

1151

Figure 6

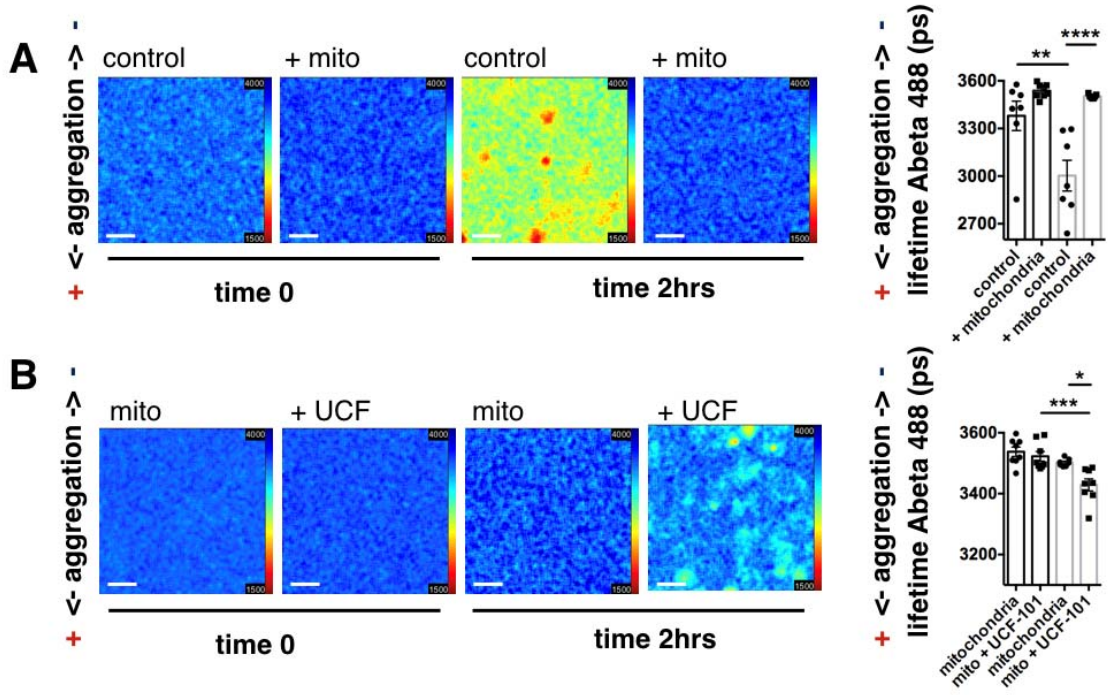

Figure EV 1

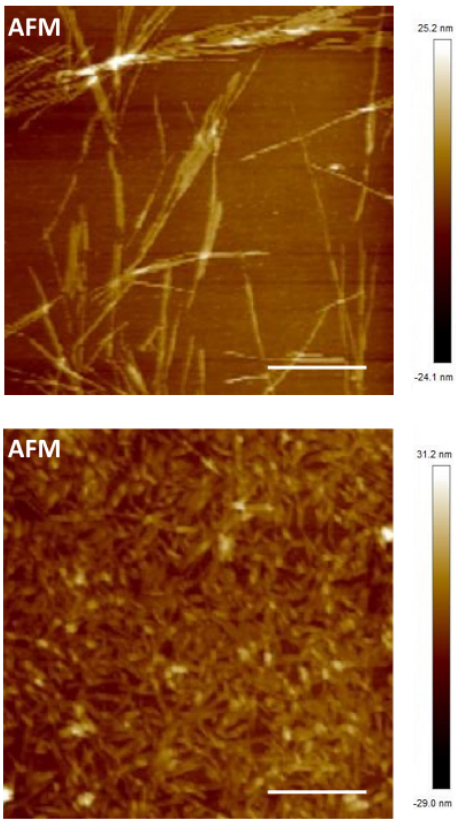

1179 **Figure EV 2**

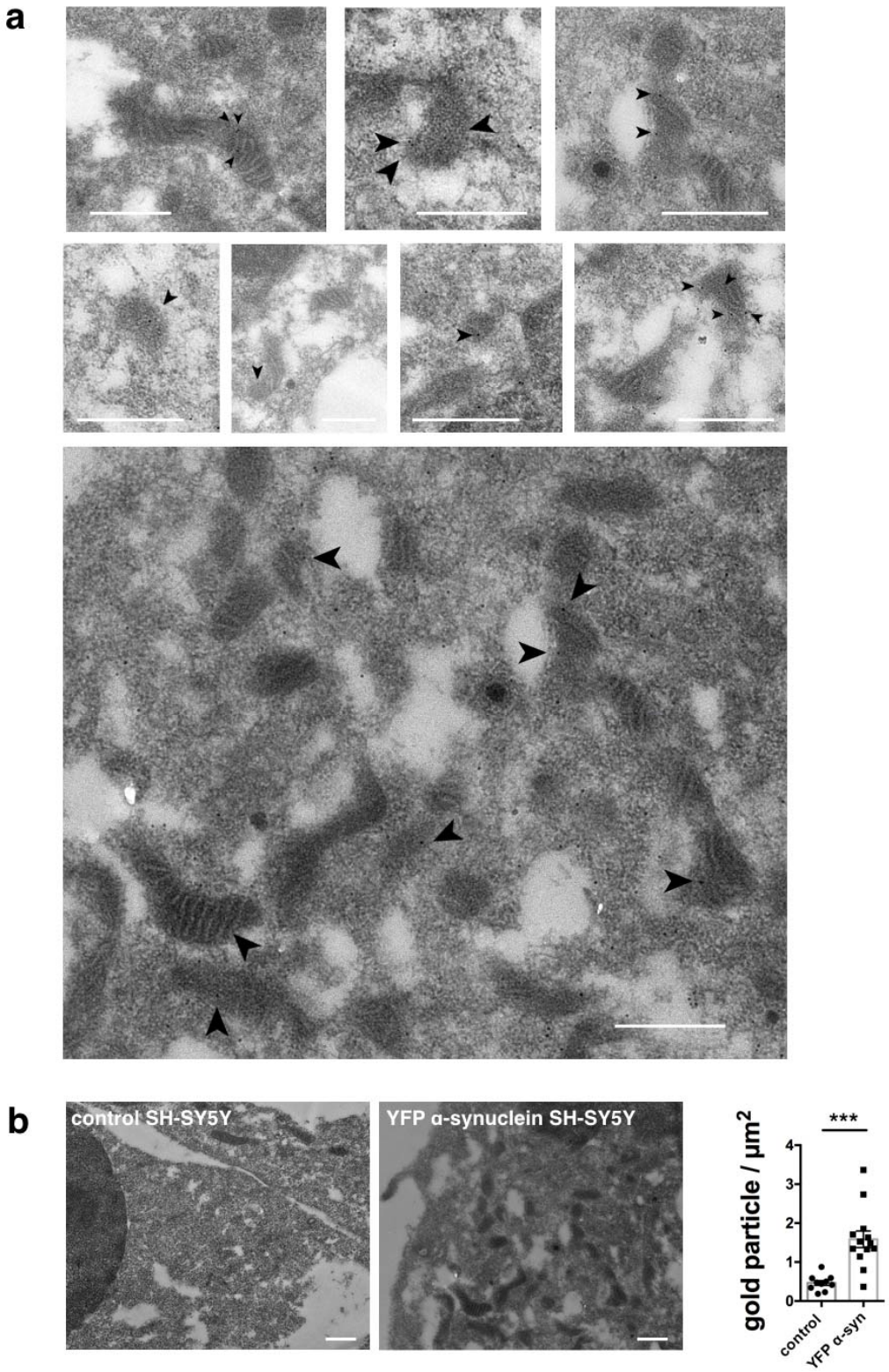

1180